

**BUCKLING OF THERMOVISCOELASTIC STRUCTURES
UNDER TEMPORAL AND SPATIAL TEMPERATURE VARIATIONS**

Thesis by
Richard M. Tsuyuki

In Partial Fulfillment of the Requirements for the Degree of
Aeronautical Engineer

Research Supported by NASA Grant NSF 1483

California Institute of Technology
Pasadena, California

1993

(Submitted January 10, 1993)

Acknowledgments

I would like to thank my advisor, Dr. Wolfgang Knauss, for much help and advice, as well as Drs. G. Ravichandran and A. Leonard for their patience and cooperation. Much appreciation also to Dr. N. O'Dowd for numerous involved mathematical discussions, and K.C. McBride for outstanding logistical support in completing this effort. Finally, thanks to Dr. James H. Starnes, technical monitor, for financial support (grant # NAG 1483) and continued discussion and encouragement.

Abstract

The problem of lateral instability of a viscoelastic in-plane loaded structure is considered in terms of thermorheologically simple materials. As an example of a generally in-plane loaded structure, we examine the simple column under axial load: Both cyclic loading is considered (with constant or in-phase variable temperature excursions) as well as the case of constant load in the presence of thermal gradients through the thickness of the structure. The latter case involves a continuous movement of the neutral axis from the center to the colder side and then back to the center.

In both cases, one finds that temperature has a very strong effect on the rate at which instabilities evolve, and under in-phase thermal cycling the critical loads are reduced compared to those at constant (elevated) temperatures. The primary effect of thermal gradients beyond that of thermally-induced rate accelerations is a rate increase occasioned by the generation of an "initial imperfection" or "structural bowing." This latter effect, which is proportional to both the temperature gradient and the coefficient of thermal expansion (presumed homogeneous in this study), can in fact be dominant. Because the coefficient of thermal expansion tends to be large for many polymeric materials, it may be necessary to take special care in lay-up design of composite structures intended for use under compressive loads in high-temperature applications. Finally, the implications for the temperature sensitivities of composites to micro-instability (fiber crimping) are also apparent from the results delineated here.

Table of Contents

1. Introduction

2. General Formulation

3. Cyclic Loading

3.1.1 Standard linear solid; isothermal case

3.1.2 Long-term stability analysis

3.1.3 Standard linear solid; in-phase thermal cycling

3.1.4 Long-term stability conditions under various load and thermal behavior

3.2 Realistic material response illustrated by PMMA

4. Effect of a Constant Thermal Gradient

4.1 Analytical results

4.2 Initial thermoelastic curvature

4.3 Quantification of failure times—design life

5. Conclusion

References

Appendix: Numerical Solution of the Displacement Equation

1. Introduction

Besides fracture, an important structural failure mode revolves around the evolution of unstable lateral deformations, often characterized as buckling. When time-dependent material behavior is involved, such as associated with polymer-based composites, this behavior depends strongly on the time history of loading and, even more so, on temperature. While one can always estimate from the relaxation or creep properties of the material lower-bound load values below which instabilities never arise [Drozdov], such bounds tend to be so low from a practical point of view that the designer is forced to use these materials at load levels at which instabilities can evolve eventually, but such that they develop on a time scale that is large compared to the anticipated life of the structure. Composites are typically used in their rigid or (near-)glassy state; it is then of interest to examine the variation in their response history as one deviates from typical low-temperature design conditions.

The problem of buckling in viscoelastic structures has been considered by several authors. Most of these deal with response under constant axial or in-plane loads. Closely attuned to the present objective, Schapery has examined the cyclic loading of viscoelastic columns under constant temperature. We shall emphasize in the present study, as did Schapery, realistically wide time ranges of material response rather than with idealized behavior. However, the present effort focuses on the derivation of stability criteria and the effect of time-varying temperature cycles.

The large time-range for buckling evolution follows from the large range of time-dependence of polymers, even when they are married to rate-insensitive reinforcements such as graphite fibers. The “stiffness” of polymers drops by a factor of 10^2 to 10^3 with time or temperature increase as the glass-transition temperature is approached. Under these circumstances it is imperative that one appreciate the limitations placed on structures by operation at elevated temperatures. While it is obviously inappropriate to allow the use of these materials uniformly at or above the glass transition, the possibility exists that they are exposed to temperature gradients in which part of the material experiences near-transition temperatures, or situations may arise when such temperatures are accidentally approached or exceeded.

With this motivation in mind we examine columns possessing thermorheologically simple material behavior subjected to two kinds of (axial) loading and thermal exposure: We consider first the case of a cyclically loaded column under constant as well as cyclically varying temperature, the latter being in phase with the loading. This problem will be first considered for the idealized material of a standard linear solid to establish certain limit behaviors. This simplified-material and exact analysis is then followed by a numerical evaluation involving realistically wide-spectrum time response following the behavior of polymethylmethacrylate (PMMA) as a model material. Along the length of the column the temperature distribution is presumed constant for all problems considered here.

The next problem concerns the effect of a thermal gradient across the thickness of the structure. Mimicking steady-state thermal conditions we consider only a linear temperature variation across the column (although a different distribution poses no additional difficulty in principle). The consequence of this thermal variation is that with time the

material exhibits varying "stiffness" across the structure, since higher temperatures are associated with faster relaxation or creep, so that the neutral axis (surface) wanders as time progresses: While being located initially and also after infinite time at the center, it is subject to an intermediate excursion towards the cold side.

Problems of time-dependent buckling instability in the absence of temperature gradients have been considered by other authors. We believe that a fair review of the state of the art in this respect is presented in references Glockner and Szyszkowski (1987) and Minahen and Knauss (1992). For our present purposes it suffices to state that in the context of the time-dependent, non-dynamic evolution of instabilities, the criterion as to when unsafe conditions have been achieved must be established through empirical arguments; in this regard we follow Minahen and Knauss (1992) and use the achievement of a predetermined lateral deflection as the criterion for failure. Also, in view of the results in this latter reference, namely that considerations of kinematically large deformations yield virtually identical results as the completely linearized analysis, we restrict ourselves here also to linear kinematics and material response.

2. General Formulation

Following developments in Minahen and Knauss (1992) we consider an initially (very slightly) deformed column, of in-plane thickness h and unit out-of-plane thickness. In anticipation of dealing with thermal gradients through the thickness and the associated motion of the neutral axis, we designate that position with respect to the center-line as $n(t)$. Let $u_0(x, t)$ denote the axial motion of the center-line, α_x the (constant) coefficient of linear thermal expansion, and $T(z)$ the temperature variation. The strain is then

$$\epsilon_x(z, t) = \frac{\partial u_0}{\partial x}(t) - [z - n(t)] \frac{\partial^2 w}{\partial x^2} + \alpha_x T(z) \quad (1)$$

along with the stress-strain relation

$$\sigma_x(z, t) = \int_{-\infty}^t E(z, t' - \xi') \frac{\partial}{\partial \xi} \epsilon_x(z, \xi) d\xi \quad (2)$$

where

$$t' - \xi' = \int_{\xi}^t \frac{d\zeta}{\phi[T(\zeta)]} \quad (3)$$

is the reduced time (difference) based on the time-temperature shift factor $\phi(T)$. Moment equilibrium then provides the integro-differential equation

$$\int_{-\frac{h}{2}}^{\frac{h}{2}} [z - n(t)] \int_{-\infty}^t E(z, t' - \xi') \frac{\partial}{\partial \xi} \left\{ \frac{\partial u_0}{\partial x}(\xi) - [z - n(\xi)] \frac{\partial^2 w}{\partial x^2} \right\} d\xi dz \quad (4)$$

$$= P [w(x, t) + w_0(x) + n(t)]$$

with $w_0(x)$ and $w(x, t)$ denoting, respectively, the small initial imperfection (when needed) and the additional time-dependent lateral deflection as illustrated in figure 1. After expanding $w_0(x)$ and $w(x, t)$ into the Fourier series

$$w(x, t) = \sum_{m=1}^{\infty} A_m(t) \sin \frac{m\pi x}{l} \quad (5)$$

and

$$w_0(x) = \sum_{m=1}^{\infty} B_m \sin \frac{m\pi x}{l} \quad (6)$$

two equations result, one governing the location of the neutral axis

$$\int_{-\frac{h}{2}}^{\frac{h}{2}} [z - n(t)] \int_{-\infty}^t E(z, t' - \xi') \frac{\partial}{\partial \xi} \left[\frac{\partial u_0}{\partial x}(\xi) \right] d\xi dz = P n(t) \quad (7)$$

and the other representing moment equilibrium

$$\left(\frac{\pi}{l}\right)^2 \int_{-\frac{h}{2}}^{\frac{h}{2}} [z - n(t)] \int_{-\infty}^t E(z, t' - \xi') \frac{\partial}{\partial \xi} \{[z - n(\xi)]A(\xi)\} d\xi dz = P [A(t) + B] \quad (8)$$

where, in anticipation of dealing only with the fundamental mode ($m = 1$) [see Minahen and Knauss (1992)], the subscripts m have been dropped.¹ Because the two problems to be considered subsequently need a somewhat different use of the last two equations, we shall deal with their applications in the specific contexts.

¹ It was shown in the work of Minahen and Knauss that, generally, of all the possible deformation modes the first one grows significantly faster than the higher ones. For this reason the first mode will dominate the deformation evolution.

3. Cyclic Loading

Before dealing with a material possessing realistic time response, we consider first the case of the standard linear solid with the intention of characterizing the typical aspects of the problem and to allow for an evaluation of the numerical scheme applied later to the situation with more realistic properties. Computational solutions require compromises in the discretization of the integration so that a check on the reliability of the scheme is at least desirable, if not mandatory, in light of earlier experience in [Minahen and Knauss (1992)]. We choose a “square wave” loading history because it approximates typical use conditions better than a sinusoidal history, but also with the expectation that a piece-wise sequential solution is possible. The results obtained in the sequel for equal on/off times are readily generalized for unequal on/off ratios with square wave loading. The thermal excursions are of the same type so that a rise in load is accompanied by a rise in temperature and unloading is accompanied by a drop in temperature without considerations of thermal delay transients (c.f. figure 2). In fact, it turns out that any piecewise-constant load history can be dealt with using the procedure developed below, such that the effects of loading functions with multiple load levels or discretized approximations of load histories which do not resemble square waves can be obtained with only slightly more effort.

3.1.1 Standard linear solid; isothermal case

Because in the present case the temperature is uniform throughout the geometry, the neutral axis remains at the center-line or midsurface. Equation (7) is thus satisfied identically

and, after normalizations in the form of

$$\begin{aligned} p(t) &\equiv \frac{P(t)}{P_e(0)}, & P_e(t) &\equiv \left(\frac{\pi}{l}\right)^2 E(t)I \\ r(t) &\equiv \frac{E(t)}{E(0)}, & \alpha(t) &\equiv \frac{A(t)}{h}, & \beta &\equiv \frac{B}{h} \end{aligned} \quad (9)$$

(8) reduces to

$$r(t')\alpha(0^+) + \int_{0^+}^t r(t' - \xi') \frac{d\alpha(\xi)}{d\xi} d\xi = p(t)[\alpha(t) + \beta] \quad (10)$$

where the relaxation behavior is characterized by

$$r(t) = r_\infty + r_1 e^{-\lambda t}; \quad r_\infty = \frac{E(\infty)}{E(0)}; \quad r_1 = 1 - r_\infty. \quad (11)$$

We effect a solution of (10) for a loading-unloading-loading cycle to show by induction that a sequential or recursive solution may be obtained. First integrate (10) across the load jump at $t = 0$ to obtain

$$\alpha(0^+) = \frac{p_0 \beta}{1 - p_0} \quad (12)$$

and then establish the lateral column motion under time-invariant axial loading. This result was given in [Minahen and Knauss, 1992] for any load level p_0 as shown in figure 3, which is valid for the first loading portion, with the explicit form for this function being given, for arbitrarily long pulse duration t , by

$$\alpha_{l1}(t) = C_1 e^{-\mu t} + C_2 \quad (13)$$

where

$$C_1 \equiv \alpha(0^+) + \frac{p_0 \beta}{p_0 - r_\infty}, \quad \mu \equiv -\lambda \frac{p_0 - r_\infty}{1 - p_0}, \quad C_2 \equiv -\frac{p_0 \beta}{p_0 - r_\infty}. \quad (14)$$

We shall refer hereafter to (13) as the *deflection function*. Integrating (10) also across the unloading jump at $t = t_0$ yields the corresponding deflection decrease

$$\Delta\alpha = -p_0[\alpha(t_0^-) + \beta]. \quad (15)$$

To obtain the deflection for the unloaded portion of the cycle we let

$$p(t) = p_0[h(t) - h(t - t_0)] \quad (16)$$

in (10), and deduce, with the aid of Laplace transformation and some tedious algebra, that during the time $t_0 < t < 2t_0$ the lateral midspan deflection is

$$\alpha_{u11}(t) = C_3 e^{-r_\infty \lambda t} \quad (17)$$

with

$$C_3 \equiv p_0 \left[(C_2 + \beta) \frac{r_1}{r_\infty} (e^{r_\infty \lambda t_0} - 1) + \frac{C_1 r_1 \lambda}{\mu - r_\infty \lambda} (1 - e^{(r_\infty \lambda - \mu)t_0}) \right]. \quad (18)$$

One follows the same procedure for the time interval $2t_0 < t < 3t_0$ and determines that during this second loading cycle,

$$\alpha_{12}(t) = C_4 e^{-\mu t} + C_2 \quad (19)$$

where

$$C_4 = \alpha_0^+ \frac{1 - r_\infty}{p_0 - r_\infty} (1 - e^{\mu t_0} + e^{2\mu t_0}) + \frac{C_3}{1 - p_0} [e^{(\mu - r_\infty \lambda)t_0} - e^{2(\mu - r_\infty \lambda)t_0}] \quad (20)$$

μ and C_2 are the same as in (14), and C_3 is defined in (18). Comparison with (13) shows that this response can be determined from the deflection under step-loading in equation (13) through a “time shift” of the form

$$\alpha_{12}(t) = C_1 e^{-\mu(t-\hat{t})} + C_2, \quad \hat{t} = \frac{1}{\mu} \ln \frac{C_4}{C_1} \quad (21)$$

which observation is also illustrated in figure 4. Because further stepwise integration becomes very cumbersome even for this simple material problem, we deduce by induction that a sequence for further load cycles may be constructed through successive determination of the (glassy) jumps at the loading and unloading times plus segments of the loading

and unloading functions, (13) and (17) respectively, such that their magnitudes match the values at the beginnings or ends of the load cycles.² In this sense, these two curves become "master curves" for the deformation during the loaded and unloaded portions of the cycles.

3.1.2 Long-term stability analysis

This term-by-term construction of the solution becomes tedious and because we are interested only in the maximum deflection at the end of each cycle we are satisfied with tracing the history of that particular parameter since it will determine the eventual failure of the structure. To this end, we consider the accumulation of the deflection over any load cycle by considering the jumps at the loading and unloading time nt_0 and $(n + 1)t_0$, as well as the change during the respective time intervals. Starting with the deflection at the end of a loading cycle, $\alpha(nt_0^-)$, we find the subsequent (downward) jump

$$\alpha(nt_0^+) = \alpha(nt_0^-) - p_0[\alpha(nt_0^-) + \beta] \quad (22)$$

the displacement at the end of the unloaded interval

$$\alpha[(n + 1)t_0^-] = \alpha(nt_0^+)e^{-r_\infty \lambda t_0} \quad (23)$$

the (upward) jump at the onset of a new loading interval

$$\alpha[(n + 1)t_0^+] = \alpha[(n + 1)t_0^-] + \frac{p_0[\alpha[(n + 1)t_0^-] + \beta]}{1 - p_0} \quad (24)$$

² This response history has also been computed numerically for comparison purposes and as a check on the algorithm used later. With 100 or 1000 time steps per cycle it was found that over the duration of 40 cycles the differences amounted to no more than 0.1%. The same result prevailed for cycles possessing fractions of the loading/unloading cycle that differed from the 50/50 example illustrated here.

and the displacement at the end of the next loading interval

$$\alpha[(n+2)t_0^-] = [\alpha[(n+1)t_0^+] - C_2]e^{-\mu t_0} + C_2. \quad (25)$$

By combining (22) through (25) one finds

$$\Delta\alpha_{\text{cycle}} \equiv \alpha[(n+2)t_0^-] - \alpha(nt_0^-) \quad (26)$$

and therefore

$$\Delta\alpha_{\text{cycle}} = [e^{-(r_\infty\lambda+\mu)t_0} - 1]\alpha(nt_0^-) + \alpha(0^+)(1 - e^{-r_\infty\lambda t_0})e^{-\mu t_0} + C_2(1 - e^{-\mu t_0}) \quad (27)$$

recalling that $\alpha(0^+)$ is given by equation (12).

It is apparent that the character of the accumulated deflections is determined by the term multiplying $\alpha(nt_0^-)$. If this term is negative, successive deflection increments decrease with time so that the total deflection tends asymptotically to an upper limit. It is negative if $(r_\infty\lambda + \mu) > 0$ which, with (14), indicates stability if

$$p_0 < p_{cr} \equiv \frac{2r_\infty}{1 + r_\infty} \quad (28)$$

in which case the maximum deflection is asymptotic (i.e., $\Delta\alpha_{\text{cycle}} = 0$) to

$$\alpha_{\text{max}}(\infty) = \frac{\alpha(0^+)(1 - e^{-r_\infty\lambda t_0})e^{-\mu t_0} + C_2(1 - e^{-\mu t_0})}{1 - e^{-(r_\infty\lambda+\mu)t_0}}. \quad (29)$$

It is clear that if $p \geq p_{cr}$ a bounded displacement is not achieved as $t \rightarrow \infty$; in fact, if $p = p_{cr}$, the displacement amplitude diverges linearly with time or number of cycles, while it grows exponentially if $p > p_{cr}$. Illustrations of these three distinct cases are given in figures 5–7. For these examples the standard linear solid model is

$$r(t) = 0.5(1 + e^{-(t/7.21\text{hrs})}). \quad (30)$$

3.1.3 Standard linear solid; in-phase thermal cycling

Because of the piecewise construction of the solution, the extension to thermal variations is simple, whether that variation is in-phase or out-of-phase. The situation for thermal cycling which is phase-shifted with respect to the loading by a fixed amount is only slightly more complicated than the case presented here, while the case of thermal cycling with a different frequency than the load cycle does not seem to lend itself to any other than a completely numerical solution. From an engineering point of view, the synchronous load and temperature variation presents the most relevant problem and is the only one considered here.

We assume that for this simple material model, a time-temperature superposition behavior such as indicated in figure 8 applies; the two shift factors corresponding to the two temperatures T_1 and T_2 are $\phi_1 = \phi(T_1)$ and $\phi_2 = \phi(T_2)$. The analysis follows identical lines of reasoning as before, except that t is replaced by the appropriate t/ϕ . Thus equations (13) and (17) become, respectively

$$\alpha_{11}(t) = C_1 e^{-(\mu/\phi_1)t} + C_2 \quad (31)$$

and

$$\alpha_{u11}(t) = p_0 \left[(C_2 + \beta) \frac{r_1}{r_\infty} (e^{r_\infty \lambda t_0} - 1) + \frac{C_1 r_1 \lambda}{\mu - r_\infty \lambda} (1 - e^{(r_\infty \lambda - \mu)t_0}) \right] e^{-(r_\infty \lambda / \phi_2)t}. \quad (32)$$

We address first the question of stable/unstable deflection growth in the presence of these temperature variations. Following the same reasoning as that which led to equations (27) and (28) one finds that (27) is replaced by

$$\Delta\alpha_{\text{cycle}} = [e^{-(r_\infty \lambda / \phi_2 + \mu / \phi_1)t_0} - 1] \alpha(nt_0^-) + \alpha(0^+) (1 - e^{-r_\infty \lambda t_0 / \phi_2}) e^{-\mu t_0 / \phi_1} + C_2 (1 - e^{-\mu t_0 / \phi_1}) \quad (33)$$

from which (28) becomes

$$p_{cr}^*(T) = \frac{r_\infty(1 + \frac{\phi_2}{\phi_1})}{\frac{\phi_2}{\phi_1} + r_\infty} \quad (34)$$

For constant temperature, equation (28) is recovered. We note that for the thermal variations considered here typically $\phi_1/\phi_2 \geq 1$ (and $r_\infty \ll 1$); as a consequence one has $p_{cr}/p_{cr}^* \leq 1$, with the implication that a load level which renders stable long-term deformations can lead to unstable growth in the presence of thermal cycling. An example of this situation is demonstrated in figure 9, where the load level for the isothermal case illustrated for the example of stable deformation growth now causes unstable growth as the temperature excursions are added. It is important to recognize, however, that it is the cyclic nature of the temperature variations that is responsible for this unstable behavior and not merely a uniform change of the temperature: In the latter case, one would merely effect an acceleration of the time scale by which the deformation is achieved. The unstable behavior in the case of the cyclic temperature variation results from the fact that during the loading portion of the cycle when the temperature is higher, deformations grow to a larger extent than they recover during the unloaded portion when the temperature is low and when the creep response is retarded.

3.1.4 Long-term stability conditions under various load and thermal behavior

As T_1/T_2 increases, ϕ_1/ϕ_2 decreases and, upon examining (34), we find that p_{cr}^* approaches r_∞ . This can be interpreted as the deflection increasing rapidly during the high-temperature loaded portions of the cycle but recovering little during the lower-temperature unloading segments. If the recovery becomes negligible, the case of no recovery is approached (i.e. time-invariant loading), so that stability is determined by the generally

very low rubbery buckling load given corresponding to r_∞ . On the other hand, as T_1/T_2 decreases, p_{cr}^* approaches unity: The retarded deflection during low-temperature loadings is recovered at an accelerated rate during unloading such that deformation does not accumulate, and only a load equal to the glassy buckling load, i.e., $p = 1$, can cause unstable deflection.

We include here also the results for the case where the loading and unloading portions of a cycle are of different durations t_1 and t_2

$$p_{cr}^{**}(T) = \frac{r_\infty(1 + \frac{t_1}{t_2} \frac{\phi_2}{\phi_1})}{\frac{t_1}{t_2} \frac{\phi_2}{\phi_1} + r_\infty}. \quad (35)$$

For constant temperature ($\phi_1 = \phi_2$) and equal loading and unloading durations ($t_1 = t_2$), equation (28) is recovered. Similar to above, limits as t_1/t_2 approach infinity or zero give values of p_{cr}^{**} of r_∞ and unity, respectively, which can be interpreted as representing cases of no-recovery continuous loading and periodic impulsive loadings.

3.2 Realistic material response illustrated by PMMA

Having dealt with the standard linear solid, primarily to establish the long-term stability boundary for the thermal cycling situation we turn to consideration of the counterpart problem but for a material with a realistically wide spectral distribution of relaxation times. As in an earlier presentation we employ the relaxation characteristics of polymethylmethacrylate (PMMA) as an exemplary material, though newer high-temperature materials will certainly possess more appropriate capabilities. However, we employ the properties of PMMA because these properties, including the time-temperature trade-off in the glassy and near-glassy domains, are well known; the same cannot be said about most

or all of the polymers typically used in the manufacture of composite materials. Although PMMA is an uncrosslinked polymer and as such does not offer a long-term equilibrium modulus, we associate such a limit with the entanglement plateau. It is not the purpose of this section to simply duplicate the earlier analysis for a different material, but to examine whether representations can be extracted from such an exercise that provides guidance for understanding qualitatively, and on a more realistic time-scale, the effect which cyclic loading can have on a thermoviscoelastic structure under constant and synchronous heating. In particular, we shall be interested in examining how the cyclic problem can be compared to that employing constant load as a reference, since the latter is readily computed approximately for realistic material behavior.

We use the relaxation modulus shown in figure 10 which represents the combined measurements by Lu (1992) and McLoughlin and Tobolsky (1952) except that we eliminate the very long-term flow regime and replace it by rubbery equilibrium behavior.³ We recognize that this relaxation behavior is not precisely that of thermoplastic-matrix composites applications but we believe it to be representative if we do not limit ourselves to fiber-dominated lay-up configurations; in any case, this statement is the more reasonable as we shall present all data and interpretations normalized by the short-time or glassy modulus. The governing integral equation (3) is evaluated numerically.

While we shall thus substitute for the relaxation or creep characteristics of the composite solid that of PMMA, with modifications as discussed above, it is imprudent to assess the behavior of carbon-reinforced polymers using the thermal expansion characteristics of

³ For computational purposes we represent the relaxation function by a series of exponentials (Prony-Dirichlet series) of 30 terms.

PMMA. The reason is that the coefficient of thermal expansion of PMMA is about two orders of magnitudes larger than that of typical fiber-reinforced materials in the fiber direction, though, transverse to the latter, the expansion may also be large by comparison [Schapery (1991)]. In order to deduce engineering-relevant information from these computations it is therefore reasonable to choose an appropriately small coefficient of axial thermal expansion and use the text value of $\alpha_x = 3 \times 10^{-6}/^\circ\text{C}$.

A note is in order on the criterion used to establish failure by buckling. Following Minahen and Knauss (1992), we use the attainment of a chosen deflection as the failure criterion. The time to failure is then the time to reach this deflection under any loading conditions. For demonstrative purposes, we may think of such a value as two or three multiples of the column thickness; we use a factor of 2.4 in this presentation.

Before turning to a comparison of the effect of a thermal gradient on the time scale of failure, we illustrate first four cases of column deflection history under cyclic loading for “realistic” material properties, namely subcritical, critical, and supercritical behavior, as well as a case for how the subcritical case can become supercritical (unstable) if thermal cycling accompanies loading. These situations are illustrated in figure 11 where the shaded area between each two curves represents the range of deformations as the column midpoint displacement increases under cyclic loading. The fourth figure in this group applies to the case of a load which in the constant temperature case is subcritical, but which becomes supercritical when the temperature accompanying the load cycle increases load-synchronously by 10°C , similar to figure 9 for the standard linear solid. We note first that for material behavior with a large range of relaxation times it is no longer reasonably possible to computationally establish whether the deflection tends toward a limit value

for very long (infinite) times. At best one observes that for supercritical loading the rate of growth increases with time, while for the critical and subcritical loading the converse seems to hold. This behavior follows from the previously developed long-term stability boundaries which are also valid for a material with realistic relaxation behavior.

It is apparent that any cyclic loading with maximal load amplitude p_0 will lead to failure after longer times than for the case when the same load p_0 acts invariantly with time; in fact, the same load which leads to eventual failure when constant may result in a long-term stable deflection when applied cyclically. On the other hand, it is of interest to examine the relative behavior between the two cases when the load in each case is normalized by its respective long-term stability boundary in such a way that the respective loads are related by

$$\left[\frac{p_0}{p_{cr}} \right]_{const} = \left[\frac{p_0}{p_{cr}^*} \right]_{cyc} . \quad (36)$$

When this is done, as shown in figures 12–14, a very close agreement between the two responses is apparent. This result indicates that, while the realistic material response to cyclic loading may be analytically difficult and computationally time-consuming, the more-easily computed constant-load case can be used, by employing the above equivalence relation, to evaluate long-term behavior. It is worth noting that this equivalence *cannot* be used in comparing time-invariant and cyclic behavior in the case of the standard linear solid. Figures 15–17 clearly reveal this lack of correspondence. Although in the critical loading case the constant-load deflection follows the average deflection under cyclic load, the other two cases show divergence. The lack of a realistic range of relaxation times does not allow the above-determined equivalence to be applied.

4. Effect of a Constant Thermal Gradient

We next consider a column loaded axially at the center-line by a *step* load of magnitude P but in the presence of a transverse thermal gradient. Along the length of the column the temperature distribution is constant. We do not include for this section an intrinsic initial imperfection, because the thermal gradient induces a lateral, stress-free deflection, which we designate by $w_0(x)$. Consider the coefficient of thermal expansion α to be a constant in the temperature range of interest.

Because of the thermoviscoelastic material behavior and the thermal gradient the effective properties vary across the thickness so that the neutral axis, located a distance $n(t)$ from the center-line, moves with time as dictated by (7). The position of the neutral axis can be determined explicitly from that equation as

$$n(t) = \frac{\int_{-\frac{h}{2}}^{\frac{h}{2}} z \int_{-\infty}^t E[t'(t, z) - \xi'(\xi, z)] \frac{\partial}{\partial \xi} \left[\frac{\partial u_0}{\partial x}(\xi) \right] d\xi dz}{\frac{P}{g} + \int_{-\frac{h}{2}}^{\frac{h}{2}} \int_{-\infty}^t E[t'(t, z) - \xi'(\xi, z)] \frac{\partial}{\partial \xi} \left[\frac{\partial u_0}{\partial x}(\xi) \right] d\xi dz} \quad (37)$$

which can be evaluated numerically. However, it is first necessary to find $\partial u_0 / \partial x$.

Considering purely axial compression of the column, force equilibrium requires

$$\int_A \sigma_x(z, t) dA = P \quad (38)$$

or

$$\int_{-\frac{h}{2}}^{\frac{h}{2}} \int_{-\infty}^t E[t'(t, z) - \xi'(\xi, z)] \frac{\partial}{\partial \xi} \left[\frac{\partial u_0}{\partial x}(\xi) \right] d\xi dz = P. \quad (39)$$

Discretization of this equation allows iterative determination of $\partial u_0 / \partial x$ by using the Newton-Raphson method. Once $\partial u_0 / \partial x$ is known, one can solve (37) for $n(t)$. Finally,

knowing $n(t)$, one solves (8) for the displacement $A(t)$ by discretization and the Newton-Raphson method.

In the case of a linear transverse temperature gradient,

$$T(z) = az + b \quad (40)$$

and employing the Prony-Dirichlet series representation

$$E(z, t) = E_\infty + \sum_{k=1}^s E_k e^{-\lambda_k t} \quad (41)$$

along with the time-temperature superposition, the relaxation modulus becomes, for any value of z ,

$$E(z, t) = E_\infty + \sum_{k=1}^s E_k e^{-\frac{\lambda_k}{\phi[T(z)]} t} \quad (42)$$

or

$$E(z, t) = \sum_{k=0}^s E_k e^{-\frac{\lambda_k}{\phi[T(z)]} t} \quad (43)$$

where E_∞ is the 0^{th} -order coefficient. At $t = 0^+$, we define

$$E_g \equiv E(z, 0^+) = E_\infty + \sum_{k=1}^s E_k. \quad (44)$$

4.1 Analytical results

In conformity with the step loading one finds [from (39)] that, immediately after load application ($t = 0^+$),

$$\int_{-\frac{h}{2}}^{\frac{h}{2}} E_g \frac{\partial u_0}{\partial x}(0^+) dz = P \quad (45)$$

or

$$\epsilon_0 \equiv \frac{\partial u_0}{\partial x}(0^+) = \frac{1}{E_g} \frac{P}{h} \quad (46)$$

and similarly for (7) and (8) that

$$n_0 \equiv n(0^+) = 0 \quad (47)$$

and

$$A(0^+) = \frac{B}{\frac{E_g I}{P} \left(\frac{\pi}{l}\right)^2 - 1}. \quad (48)$$

For the case that the column reaches a stable equilibrium at large times, we can determine the long-term results by observing that $E(z, t) \rightarrow E_\infty$ as $t \rightarrow \infty$. Then (39) becomes

$$E_\infty \int_{-\frac{h}{2}}^{\frac{h}{2}} \int_{-\infty}^t \frac{\partial}{\partial \xi} \left\{ \frac{\partial u_0}{\partial x}(\xi) \right\} d\xi dz = P \quad (49)$$

or

$$\epsilon_\infty \equiv \frac{\partial u_0}{\partial x} \Big|_\infty = \frac{1}{E_\infty} \frac{P}{h}. \quad (50)$$

Similarly, (37) leads to

$$n_\infty \equiv n(\infty) = 0 \quad (51)$$

and finally, (8) gives

$$A(\infty) = \frac{B}{\frac{E_\infty I}{P} \left(\frac{\pi}{l}\right)^2 - 1}. \quad (52)$$

We next evaluate the stability regimes of the column, following Minahen and Knauss (1992). We rewrite (48) and (52) as

$$A(0^+) = \frac{PB}{P_{cr}^0 - P} \quad ; \quad P_{cr}^0 \equiv E_g I \left(\frac{\pi}{l}\right)^2 \quad (53)$$

and

$$A(\infty) = \frac{PB}{P_{cr}^\infty - P} \quad ; \quad P_{cr}^\infty \equiv E_\infty I \left(\frac{\pi}{l}\right)^2. \quad (54)$$

P_{cr}^0 and P_{cr}^∞ are the Euler buckling loads based on the instantaneous (glassy) and long-term (rubbery) moduli, respectively, and if P approaches these values from below, the glassy and long-term responses, respectively, become unbounded. This establishes three stability regimes. If the load is less than P_{cr}^∞ (54), the deflection eventually tends to the value given by (52). If the load exceeds P_{cr}^0 (53), the column buckles instantaneously. Finally, if the load level falls between these limits, the deflection grows gradually in an unbounded manner. This is illustrated in figure 18, where the column response of a load at 1% *below* P_{cr}^∞ is illustrated; the “supercritical” load is one percent *above* that critical load.

4.2 Initial thermoelastic curvature

The initial deformation of the column follows from the thermal gradient [Timoshenko and Goodier (1987)]. We begin with an unloaded column possessing thermal coefficients of expansion α_x , α_y , and α_z (as in an orthotropic material), as shown in figure 19. The solution is found by treating the column as if it were composed of *separate* elements of differential thickness in the transverse direction and applying a compressive stress to each element to suppress thermal expansion in the longitudinal direction. We then apply opposing forces at the ends to make the ends stress-free. St.-Venant’s Principle allows the resulting stresses to be calculated away from the ends of the column without requiring the full solution. The superposition of these stresses for the longitudinal direction is then

$$\begin{aligned}
 \hat{\sigma}_x &= -E\alpha_x T(\hat{z}) + \frac{1}{h} \int_{-\frac{h}{2}}^{\frac{h}{2}} E\alpha_x T(\hat{z}) d\hat{z} + \frac{12\hat{z}}{h^3} \int_{-\frac{h}{2}}^{\frac{h}{2}} E\alpha_x T(\hat{z}) \hat{z} d\hat{z} \\
 &= -E\alpha_x (a\hat{z} + b) + \frac{1}{h} \int_{-\frac{h}{2}}^{\frac{h}{2}} E\alpha_x (a\hat{z} + b) d\hat{z} + \frac{12\hat{z}}{h^3} \int_{-\frac{h}{2}}^{\frac{h}{2}} E\alpha_x (a\hat{z} + b) \hat{z} d\hat{z} \quad (55) \\
 &= -E\alpha_x (a\hat{z} + b) + E\alpha_x b + E\alpha_x a\hat{z} \\
 &= 0.
 \end{aligned}$$

One has the following strain equations:

$$\begin{aligned}\hat{\epsilon}_x &= \alpha_x(a\hat{z} + b), & \hat{\epsilon}_y &= \alpha_y(a\hat{z} + b), & \hat{\epsilon}_z &= \alpha_z(a\hat{z} + b) \\ \hat{\epsilon}_{xy} &= \hat{\epsilon}_{xz} = \hat{\epsilon}_{yz} = 0\end{aligned}\tag{56}$$

and the resulting displacements:

$$\begin{aligned}\hat{u}_x &= \alpha_x(a\hat{z} + b)\hat{x} + d(\hat{y}, \hat{z}) \\ \hat{u}_y &= \alpha_y(a\hat{z} + b)\hat{y} + e(\hat{x}, \hat{z}). \\ \hat{u}_z &= \alpha_z\left(\frac{a}{2}\hat{z}^2 + b\hat{z}\right) + f(\hat{x}, \hat{y})\end{aligned}\tag{57}$$

By \hat{y} -symmetry, $e(\hat{x}, \hat{z}) = 0$, and if we set $u_x = 0$ at $\hat{x} = 0$ then $d(\hat{y}, \hat{z}) = 0$. Knowing the shearing strains to be zero, we can find $f(\hat{x}, \hat{y})$ and thus

$$\hat{u}_z = \alpha_z\left(\frac{a}{2}\hat{z}^2 + b\hat{z}\right) - \frac{a}{2}(\alpha_x\hat{x}^2 + \alpha_y\hat{y}^2) + \text{const.}\tag{58}$$

We therefore have

$$w_0(\hat{x}) \approx -\frac{1}{2}\alpha_x a\hat{x}^2 + \text{const.}\tag{59}$$

Now a transformation is made, from the \hat{x} , \hat{y} , \hat{z} coordinates of figure 19 to x , y , z coordinates as in figure 1; the origin is moved to the end of the column. The constant is adjusted to satisfy the boundary condition that $w_0(x) = 0$ at $x = 0$. Then

$$w_0(x) = -\frac{1}{2}\alpha_x a \left[\left(x - \frac{l}{2}\right)^2 - \frac{l^2}{4} \right].\tag{60}$$

We express w_0 in the form of a Fourier series:

$$w_0(x) = \sum_{m=1}^{\infty} B_m \sin \frac{m\pi x}{l}\tag{61}$$

in which case

$$B_m = -\frac{2}{l} \int_0^l \frac{1}{2} \alpha_x a \left[\left(x - \frac{l}{2} \right)^2 - \frac{l^2}{4} \right] \sin \frac{m\pi x}{l} dx \quad (62)$$

$$B_m = \begin{cases} \frac{4\alpha_x a l^2}{(m\pi)^3} & \text{if } m \text{ odd;} \\ 0 & \text{if } m \text{ even.} \end{cases} \quad (63)$$

In particular, we have

$$B_1 = \frac{4\alpha_x a l^2}{\pi^3} \quad (64)$$

and generally,

$$B_m = \frac{B_1}{m^3} \quad (65)$$

so that a one-term approximation with B_1 alone is not unreasonable for our present purposes.

4.3 Quantification of failure times—design life

As stated in the Introduction, the objective of this study is the determination of the time-scale within which a structure will fail by “buckling.” As in earlier studies [Minahen and Knauss, (1992)], the time-dependent problem of lateral structural deflections is characterized by an evolutionary process from a small initial imperfection rather than a sudden response as in the elastic case. As a consequence it is necessary to define, for engineering purposes, a magnitude of (maximum) deflection which is considered to constitute structural failure. As previously stated, we choose a deflection of 2.4 times the column thickness h as the criterion of failure, and determine the (failure) time to achieve this value as a function of various temperature gradients. The example geometry is a column 500 mm long and 6.35 mm thick possessing the PMMA properties given in figures 8 and 10; also, as discussed before we choose a coefficient of thermal expansion that is commensurate with typical values for composites [Tsai and Hahn (1980)].

Applying this failure criterion, *design-life curves* are obtained, by varying the end load between zero and the glassy buckling load and plotting the load values (normalized by the glassy buckling load) versus the design lifetime. Figure 20 shows the results of computations for several temperature gradients: the “cold” side is held at 30°C and the gradient difference is as indicated in the figure. Because of the highly nonlinear character of the time-temperature relation there appears to be no way to normalize these data into a more systematic context. In an attempt to condense the information we plot the same characteristics but shifted (using the time-temperature shift factor given in figure 8) according to the average temperature for each case; these plots are shown in figure 21. Beyond this representation it appears impossible to cast this data into a form that is more universally descriptive. It is obvious in either representation that because of the very strong temperature dependence of the rheological properties of the polymer the time-response of the instability process is similarly sensitive to thermal variations.

The lack of a universally simple description makes the estimation of failure times subject to large (conservative) bounds. We discuss next certain invariant aspects of this estimation process. In figure 21 we have included the results for a constant temperature and note that if the temperature changes uniformly across the column this curve shifts according to the shift factor given in figure 8. Moreover, it has been shown by Minahen and Knauss (1992) that for realistic material properties these curves are well-represented through the function of the relaxation modulus when the argument of that function contains a factor multiplying the time, which factor depends on the initial imperfection. In the present case that factor would be proportional to the temperature gradient and the coefficient of thermal expansion.

We note that the response of the column must lie between curves computed for constant temperatures (isothermal curves) corresponding to the cold and hot sides. Certainly, the shortest failure time is estimated for the situation when the whole column is at the highest temperature. Using the relaxation function to conservatively estimate the design life of a column, it appears that one attains a more reasonable estimate than the highest and lowest temperatures would allow if one compares the relaxation modulus shifted to the average temperature. At times other than very short ones the estimation based on the constant high temperature is very conservative, in fact about three orders of magnitude. Simultaneously it is clear that a less conservative estimate for some load levels may not be conservative for others, especially the high loads. At low load levels of less than one-tenth of the glassy buckling load even the isothermal estimate for the average temperature is conservative relative to the gradient response. It is believed that this excessive conservatism poses no problem because it is seldom of interest to deal with such low "buckling" loads.

While the present estimation process is indeed very conservative, it should be pointed out that it is correspondingly simple. If closer estimates than these are required, there appears to be no other way than to compute the response from (8).

5. Conclusion

The evolution of unstable lateral deformations in a thermoviscoelastic column has been investigated under a variety of loading conditions, including cyclic loading with synchronous temperature excursions, as well as time-invariant loading while subject to a transverse temperature gradient. Stability analysis in the cyclic loading case indicates that, while such loading under isothermal conditions leads to stable long-term deflections at loads greater than the rubbery buckling load (and therefore the long-term stability limit for constant loading), the addition of temperature cycling can induce unstable long-term deflection in cases with otherwise subcritical load levels, even with relatively small temperature changes. Evaluation of the behavior of a material with a realistic time-response spectrum as represented by that of PMMA leads to the conclusion that the envelope of deflections of a realistic material under cyclic loading can be approximated by the response to constant loading when an appropriate equivalent load normalization is used.

Failure-time characterization through the use of the design life concept indicates that the normalized, temperature-shifted relaxation modulus can be used to conservatively estimate the response of a viscoelastic column under constant load in the presence of a thermal gradient. A shift of the relaxation modulus corresponding to the maximum temperature of the column provides an estimate of the design life at loads approaching the glassy buckling load. For loads less than 10% of the glassy buckling load, perhaps less likely to be seen in engineering practice, a shift corresponding to the average temperature of the column is perhaps a closer, while still conservative, estimate.

This study has been conducted on a macroscopic level, but a last word concerning compar-

ison to the local fiber buckling case is in order. Indeed the results should be applicable in some sense to the localized phenomena, for, while the boundary conditions differ, the essential aspects of the time-dependence and subsequent response do not. It should be noted that the “initial imperfection” used here is entirely due to the thermoelastic expansion of the material, and, assuming a positive coefficient, this will always result in the outside of the “bowing” being the hot side of the column, and the hot (accelerated time-response) side therefore being in tension due to the end loading. However, if a specific case arises where the heating is coupled with some transverse loading such that this tendency is overcome and the bowing reverses, ending up with the hot side in compression, the local fiber buckling/crimping becomes a much more critical issue, due to the decreasing stiffness in this area. In the majority of cases likely to be encountered in real-life application, however, the “hot-side-out” assumption is adequate.

References

- Arnold, S.M., (1987) "Effects of State Recovery on Creep Buckling Induced by Thermo-mechanical Loading," Ph.D. Thesis, University of Akron, Akron, Ohio
- Bodner, S.R., (1991) "A Lower Bound on Bifurcation Buckling of Viscoplastic Structures," ASME Winter Annual Meeting.
- Distefano, J.N., (1965) "Creep Buckling of Slender Columns," *Journal of the Structural Division, ASCE*, 91, No. 3, p. 127.
- Drozdov, A., (1991) Personal Communications and (1) "Stability of Rods of Nonuniform-Aging Viscoelastic Material," *Mechanics of Solids*, 1984, 2, pp. 176-186, (co-authors: V.B. Kolmanovskii, V.D. Potapov). (2) "Stability of Beams Made of a Non-Homogeneous, Aging, Viscoelastic Material," *Dokl. Akad. Nauk Arm SSR*, 1984, 78(3), pp. 117-121, (co-authors: V.B. Kolmanovskii, V.D. Potapov). [in Russian]
- Glockner, P.G. and Szyszkowski, W., (1987) "On the Stability of Columns Made of Time Dependent Materials," in *Civil Engineering Practice* Vol. 1, (Structures) Chapter 23, ed. P.N. Cheremisinoff, N.P. Cheremisinoff and S.L. Cheng.
- Hilton, H.H., (1952) "Creep Collapse of Viscoelastic Columns with Initial Curvatures," *Journal of the Aeronautical Sciences*, 19, p. 844.

Hoff, N.J., (1956) "Creep Buckling," *Aeronautical Quarterly*, 7, p. 1.

Huang, N.C., (1976) "Creep Buckling of Imperfect Columns," *Journal of Applied Mechanics* E43, No. 1, p. 131.

Kempner, J., (1962) "Viscoelastic Buckling," in *Handbook of Engineering Mechanics* ed. F. Flügge, McGraw-Hill Book Company

Lu, H., (1992) Personal Communications, California Institute of Technology

McLoughlin, J.R. and Tobolsky, A.V., (1952) "The Elastic Behavior of Polymethylmethacrylate," *Journal of Colloid Science* 7 p 555

Minahen, T.M. and Knauss, W.G., (1993) "Creep Buckling of Viscoelastic Structures," *International Journal of Solids and Structures*, Vol. 30, No. 8, pp. 1075-1092.

Salchev, L.Z. and Williams, J.G., (1969) "Bending and Buckling Phenomena in Thermoplastic Beams," *Plastics and Polymers*, 37, p. 159.

Schapery, R.A., (1991) "Analysis of Local Buckling in Viscoelastic Composites," presentation at the *IUTAM Symposium on Local Mechanics Concepts for Composite Material Systems* VPI and State University

Timoshenko, S.P. and Goodier, J.N., (1987) *Theory of Elasticity*. McGraw Hill Book Company, New York, NY

Tsai, S.W. and Hahn, H.T., (1980) *Introduction to Composite Materials*. Technomic Publishing Company, Westport, CT

Appendix: Numerical Solution of the Displacement Equation

(8) can be solved by a straightforward numerical procedure with a Newton-Raphson approach. A special recursive relation is defined in order to facilitate time-stepping without having to preserve previous values of parameters for the convolution. This numerical methodology is also used to solve (7) and (11); here we only give the details for the solution of (8). We recast (8) in Riemann form and define the function

$$\begin{aligned}
 F(t) &= 0 \\
 &= \left(\frac{m\pi}{l}\right)^2 \int_{-\frac{l}{2}}^{\frac{l}{2}} [z - n(t)] \left\{ [z - n(0^+)] A_m(0^+) E(z, t) \right. \\
 &\quad \left. + \int_{0^+}^t E(z, t - \xi) \frac{\partial}{\partial \xi} \{ [z - n(\xi)] A_m(\xi) \} d\xi \right\} dz \\
 &\quad - P [A_m(t) + B_m].
 \end{aligned}$$

We then discretize as follows:

$$\begin{aligned}
 F(t_r) &= F_r \\
 &= \left(\frac{m\pi}{l}\right)^2 \sum_{i=1}^q [z_i - n(t_r)] \left\{ [z_i - n(0^+)] A_m(0^+) E(z_i, t_r) \right. \\
 &\quad \left. + \sum_{j=1}^r E(z_i, t_r - t_{j-1}) \frac{\Delta \{ [z_i - n(t_j)] A_m(t_j) \}}{\Delta t} \Delta t \right\} \Delta z \\
 &\quad - P [A_m(t_r) + B_m].
 \end{aligned}$$

Using (15), the previously developed expression for $E(z, t)$,

$$\begin{aligned}
 F_r &= \left(\frac{m\pi}{l}\right)^2 \sum_{i=1}^q [z_i - n(t_r)] \left\{ [z_i - n(0^+)] A_m(0^+) \sum_{k=0}^s E_k e^{-\frac{\lambda_k}{\phi(z_i)} t_r} \right. \\
 &\quad \left. + \sum_{j=1}^r \sum_{k=0}^s E_k e^{-\frac{\lambda_k}{\phi(z_i)} (t_r - t_{j-1})} \Delta \{ [z_i - n(t_j)] A_m(t_j) \} \right\} \Delta z \\
 &\quad - P [A_m(t_r) + B_m].
 \end{aligned}$$

Let

$$G_r^{k,i} = \sum_{j=1}^r E_k e^{-\frac{\lambda_k}{\phi(z_i)} (t_r - t_{j-1})} \Delta \{ [z_i - n(t_j)] A_m(t_j) \}$$

so that

$$F_r = \left(\frac{m\pi}{l}\right)^2 \sum_{i=1}^q [z_i - n(t_r)] \left\{ [z_i - n(0^+)] A_m(0^+) \sum_{k=0}^s E_k e^{-\frac{\lambda_k}{\phi(z_i)} t_r} + \sum_{k=0}^s G_r^{k,i} \right\} \Delta z - P [A_m(t_r) + B_m].$$

Then, pulling out the $j = r$ term,

$$\begin{aligned} G_r^{k,i} &= E_k e^{-\frac{\lambda_k}{\phi(z_i)} \Delta t} \Delta \{ [z_i - n(t_r)] A_m(t_r) \} \\ &+ \sum_{j=1}^{r-1} E_k e^{-\frac{\lambda_k}{\phi(z_i)} (t_r - t_{j-1})} \Delta \{ [z_i - n(t_j)] A_m(t_j) \} \\ &= E_k e^{-\frac{\lambda_k}{\phi(z_i)} \Delta t} \Delta \{ [z_i - n(t_r)] A_m(t_r) \} \\ &+ e^{-\frac{\lambda_k}{\phi(z_i)} \Delta t} \sum_{j=1}^{r-1} E_k e^{-\frac{\lambda_k}{\phi(z_i)} (t_{r-1} - t_{j-1})} \Delta \{ [z_i - n(t_j)] A_m(t_j) \} \end{aligned}$$

and the summation is now equal to the previous value of G :

$$\begin{aligned} G_r^{k,i} &= E_k e^{-\frac{\lambda_k}{\phi(z_i)} \Delta t} \Delta \{ [z_i - n(t_r)] A_m(t_r) \} \\ &+ e^{-\frac{\lambda_k}{\phi(z_i)} \Delta t} G_{r-1}^{k,i}. \end{aligned}$$

This recursive relation allows solution of the equation at successive time steps without having to retain solutions for all prior times. We can also calculate

$$\frac{\partial F_r}{\partial A_m} = \left(\frac{m\pi}{l}\right)^2 \sum_{i=1}^q [z_i - n(t_r)] \sum_{k=0}^s E_k e^{-\frac{\lambda_k}{\phi(z_i)} \Delta t} [z_i - n(t_r)] \Delta z - P.$$

Then, using the Newton-Raphson method, where A'_m is the current guess for A_m and A''_m is the updated guess,

$$\begin{aligned} A''_m &= A'_m + \Delta A_m \\ F_r(A''_m) &= F_r(A'_m + \Delta A_m) \\ &= F_r(A'_m) + \frac{\partial F_r(A'_m)}{\partial A_m} \Delta A_m + \dots \end{aligned}$$

We wish to find $F_r = 0$, so

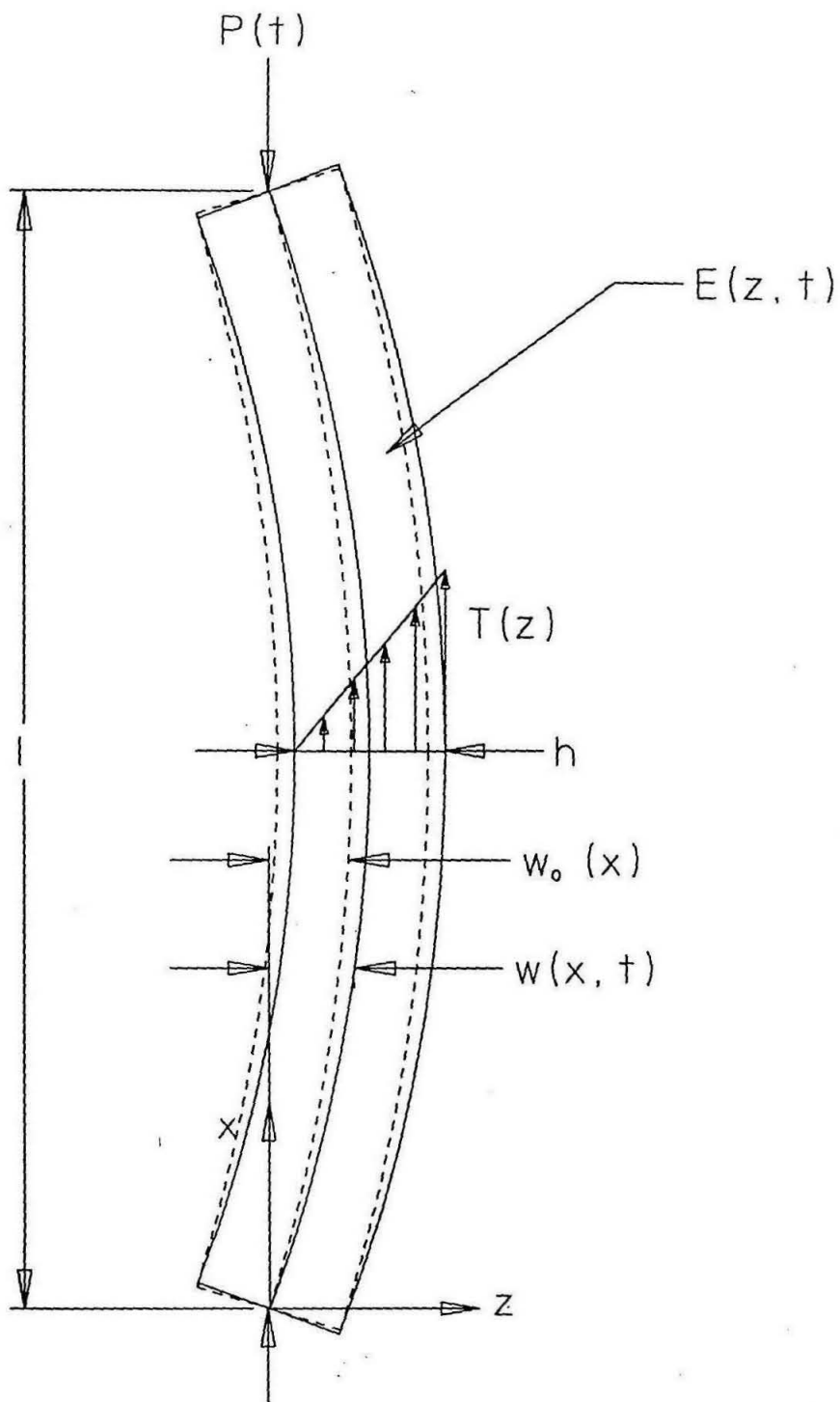
$$0 = F_r(A'_m) + \frac{\partial F_r(A'_m)}{\partial A_m} \Delta A_m + \dots$$

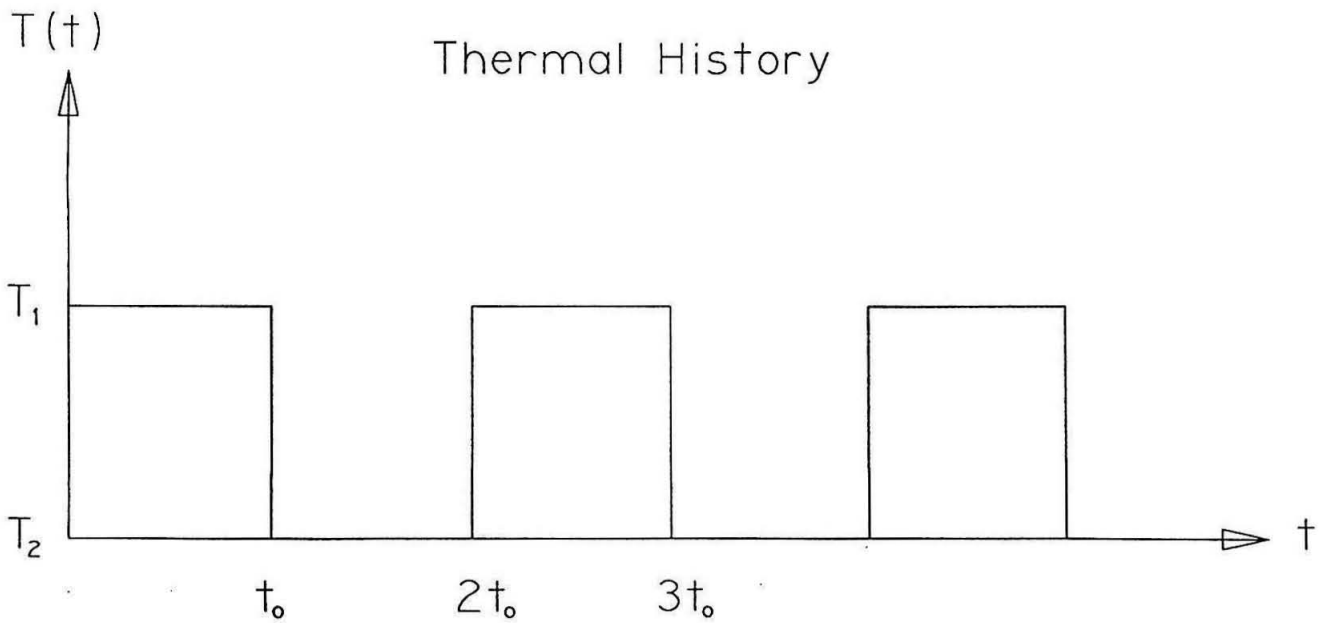
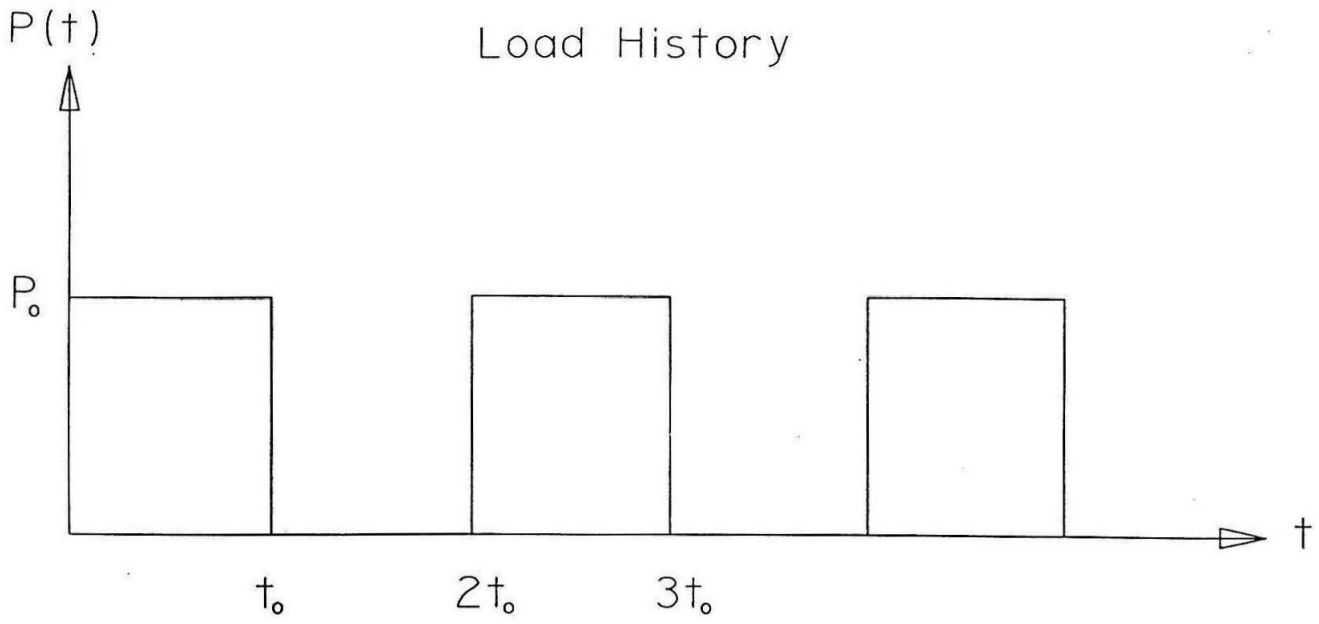
Therefore we approximate:

$$\Delta A_m = -\frac{F_r(A'_m)}{\partial F_r / \partial A_m}.$$

Figure Captions

1. Viscoelastic Column Under End Load
2. Cyclic Loading
3. Column Response Under Step Load: Deflection Function
4. Illustration of the Piece-wise Procedure
5. Subcritical Load Case, Standard Linear Solid
6. Critical Load Case, Standard Linear Solid
7. Supercritical Load Case, Standard Linear Solid
8. Time-Temperature Shift Factor for PMMA
9. Effect of Temperature Cycling, Standard Linear Solid
10. Relaxation Modulus of PMMA at 100°C
11. Realistic Deflection Response
12. Comparison of Cyclic and Constant Loading, PMMA, Subcritical Load
13. Comparison of Cyclic and Constant Loading, PMMA, Critical Load
14. Comparison of Cyclic and Constant Loading, PMMA, Supercritical Load
15. Comparison of Cyclic and Constant Loading, SLS, Subcritical Load
16. Comparison of Cyclic and Constant Loading, SLS, Critical Load
17. Comparison of Cyclic and Constant Loading, SLS, Supercritical Load
18. Illustration of Critical Load
19. Elastic Column Under Thermal Gradient
20. Design Lifetimes for Different Temperature Gradients
21. Shifted Designs Lifetimes for Different Temperature Gradients
22. Design Lifetime Comparison With Modulus Curves

**Figure 1**

**Figure 2**

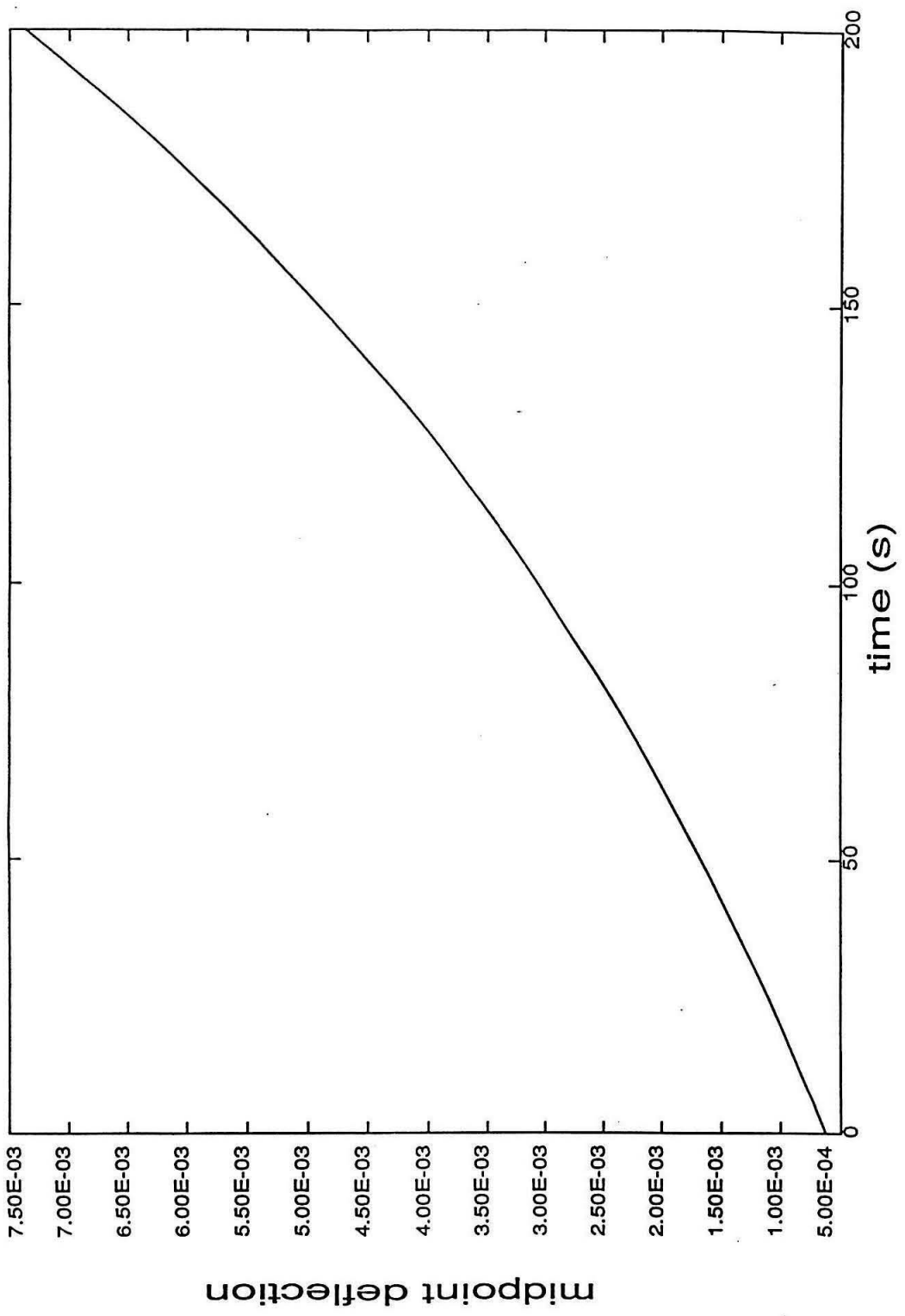
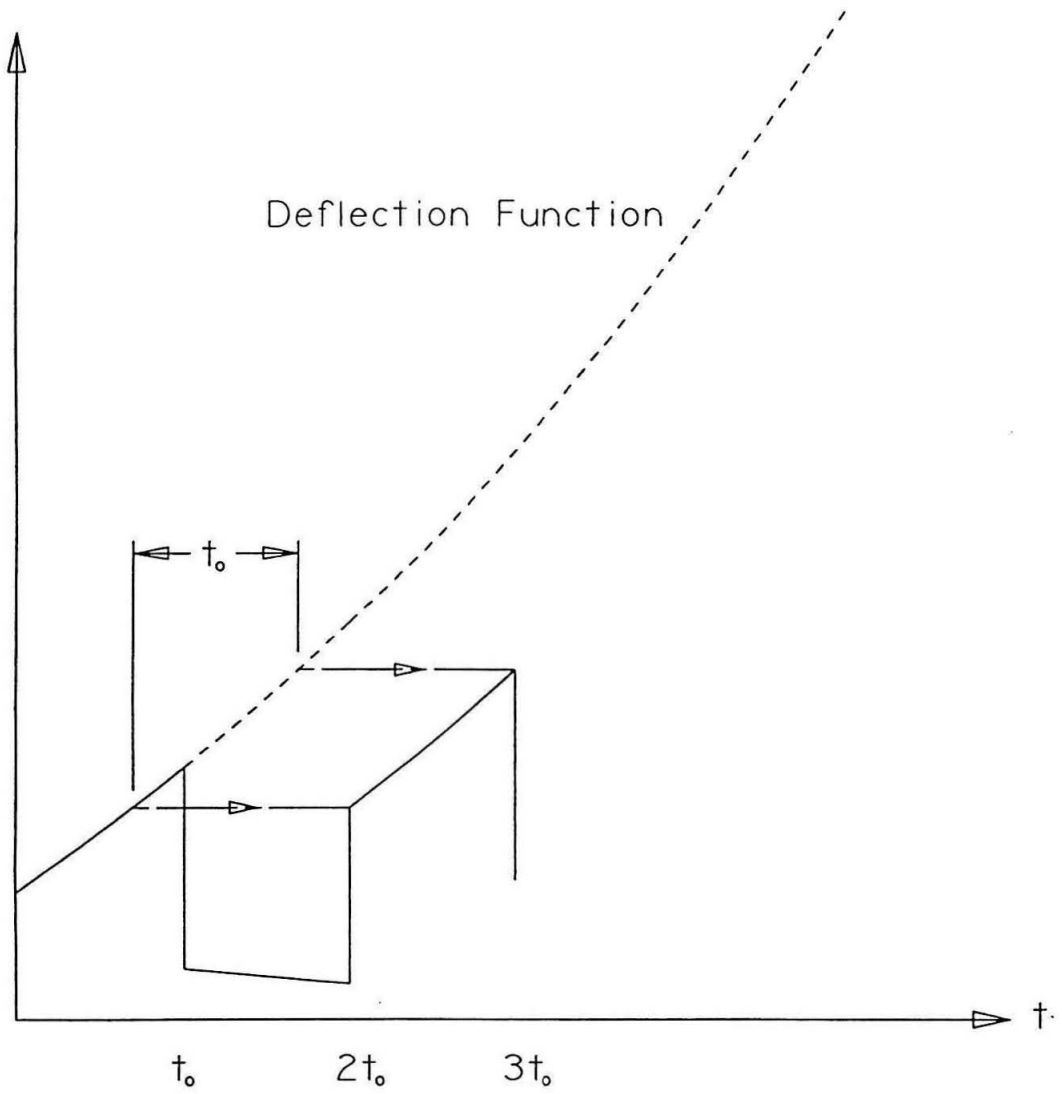


Figure 3

**Figure 4**

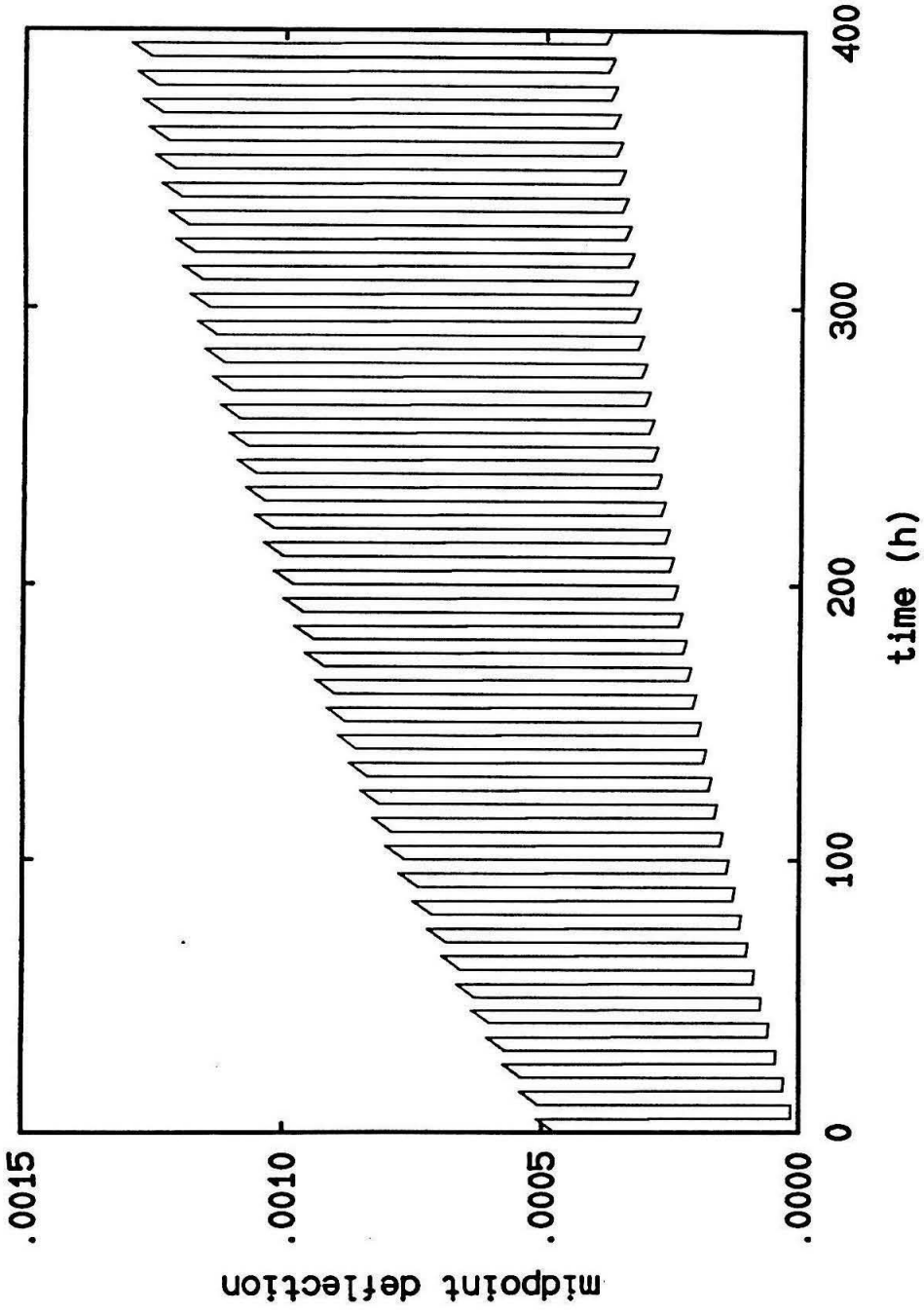


Figure 5

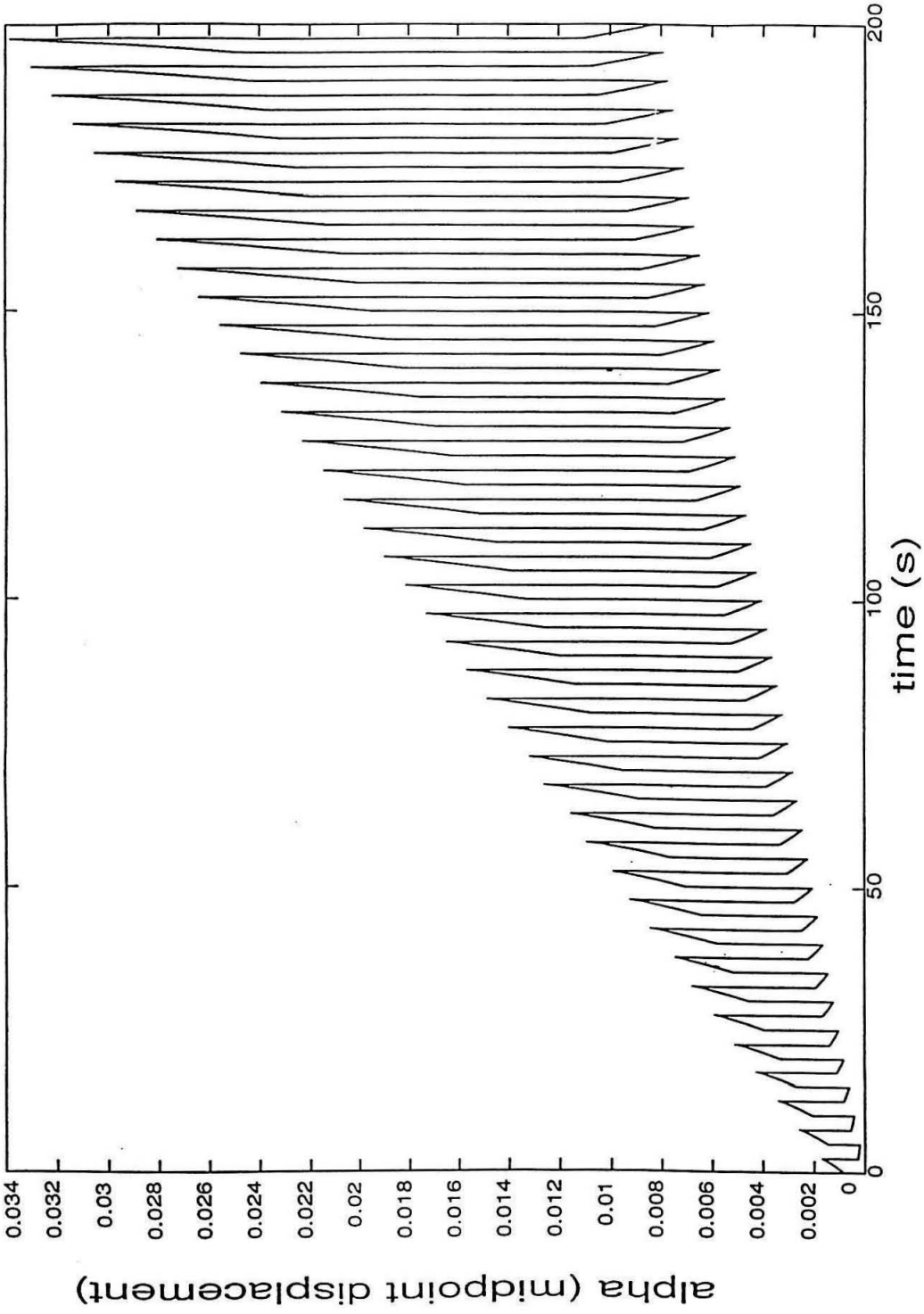


Figure 6

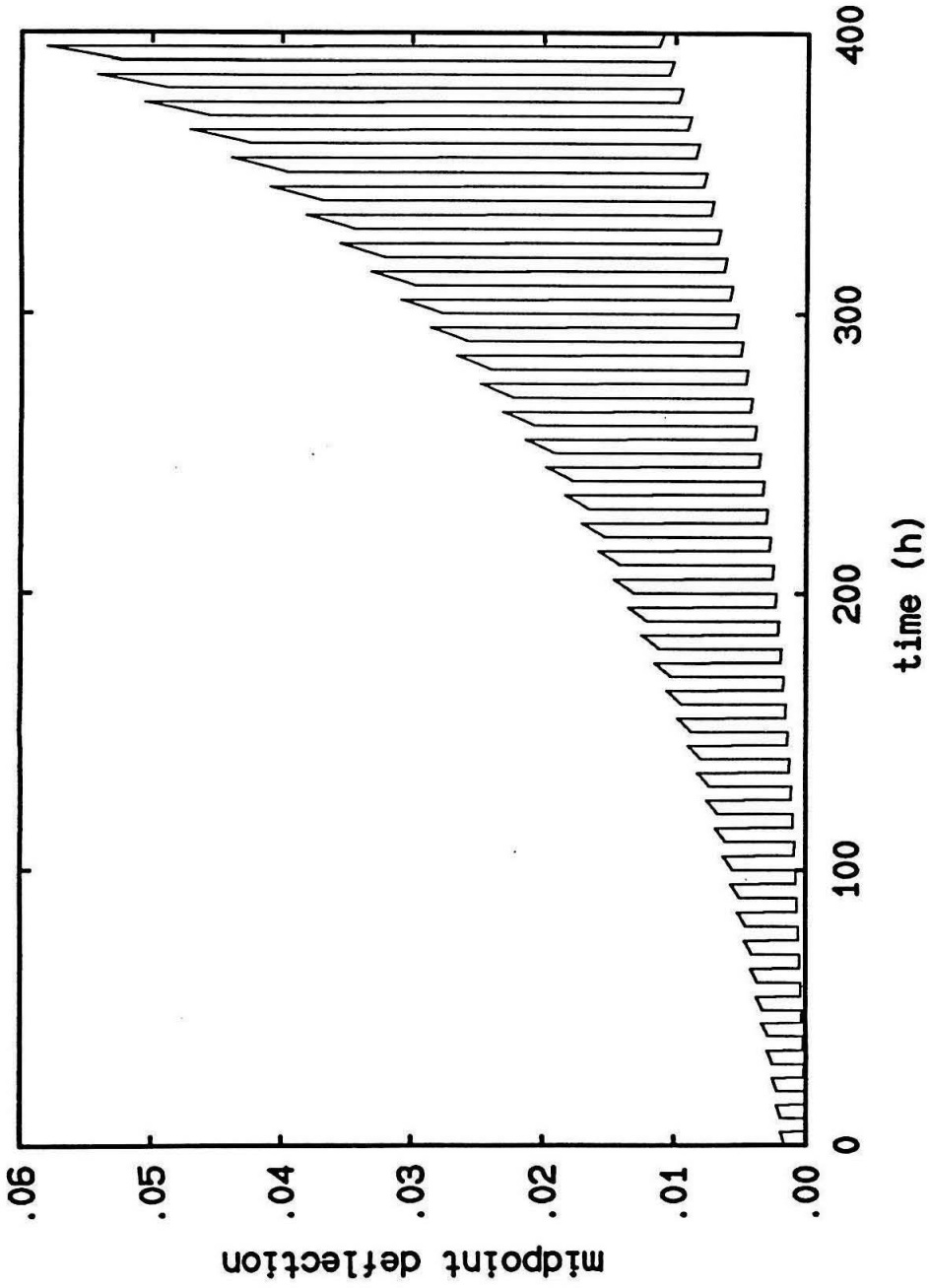


Figure 7

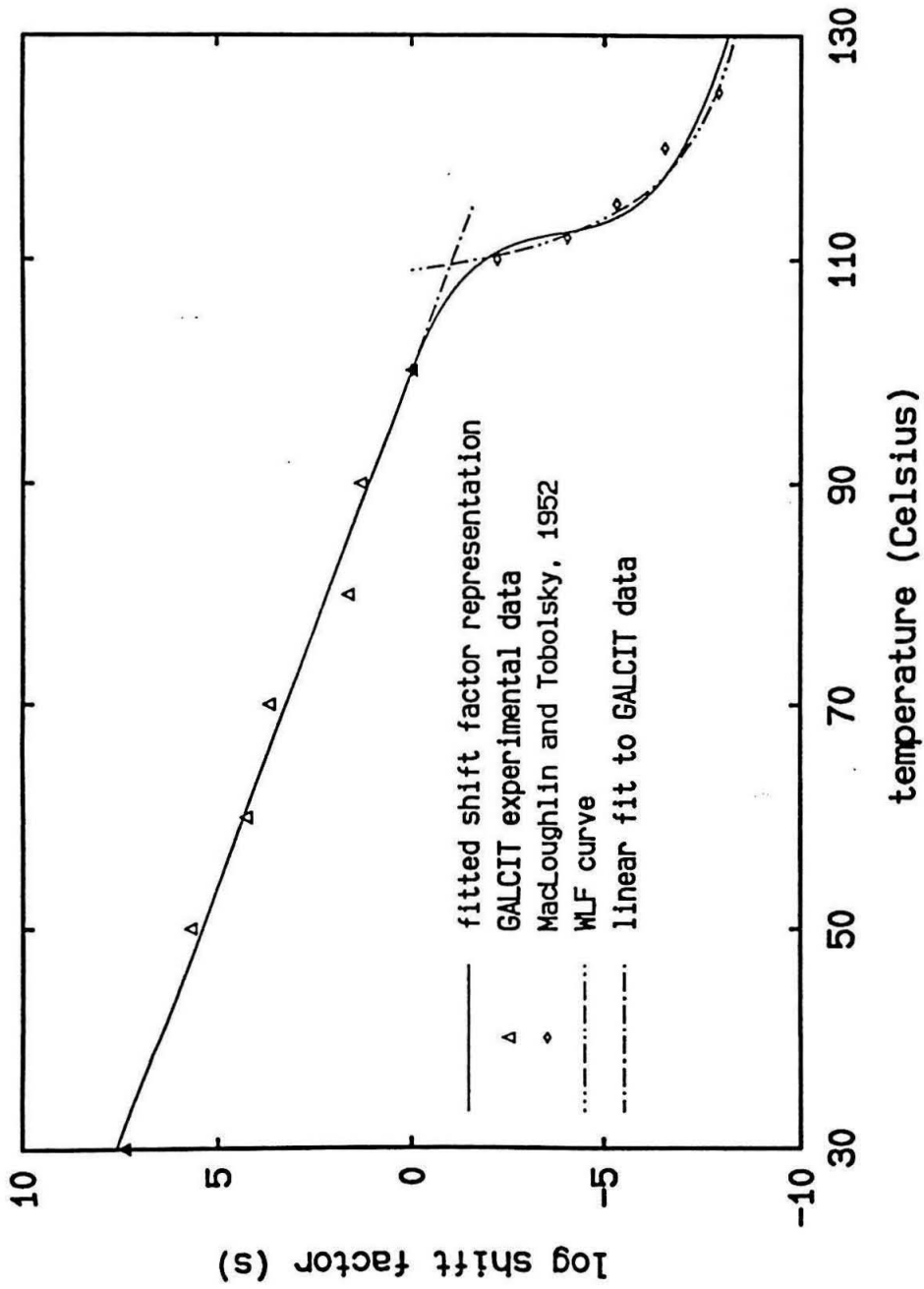


Figure 8

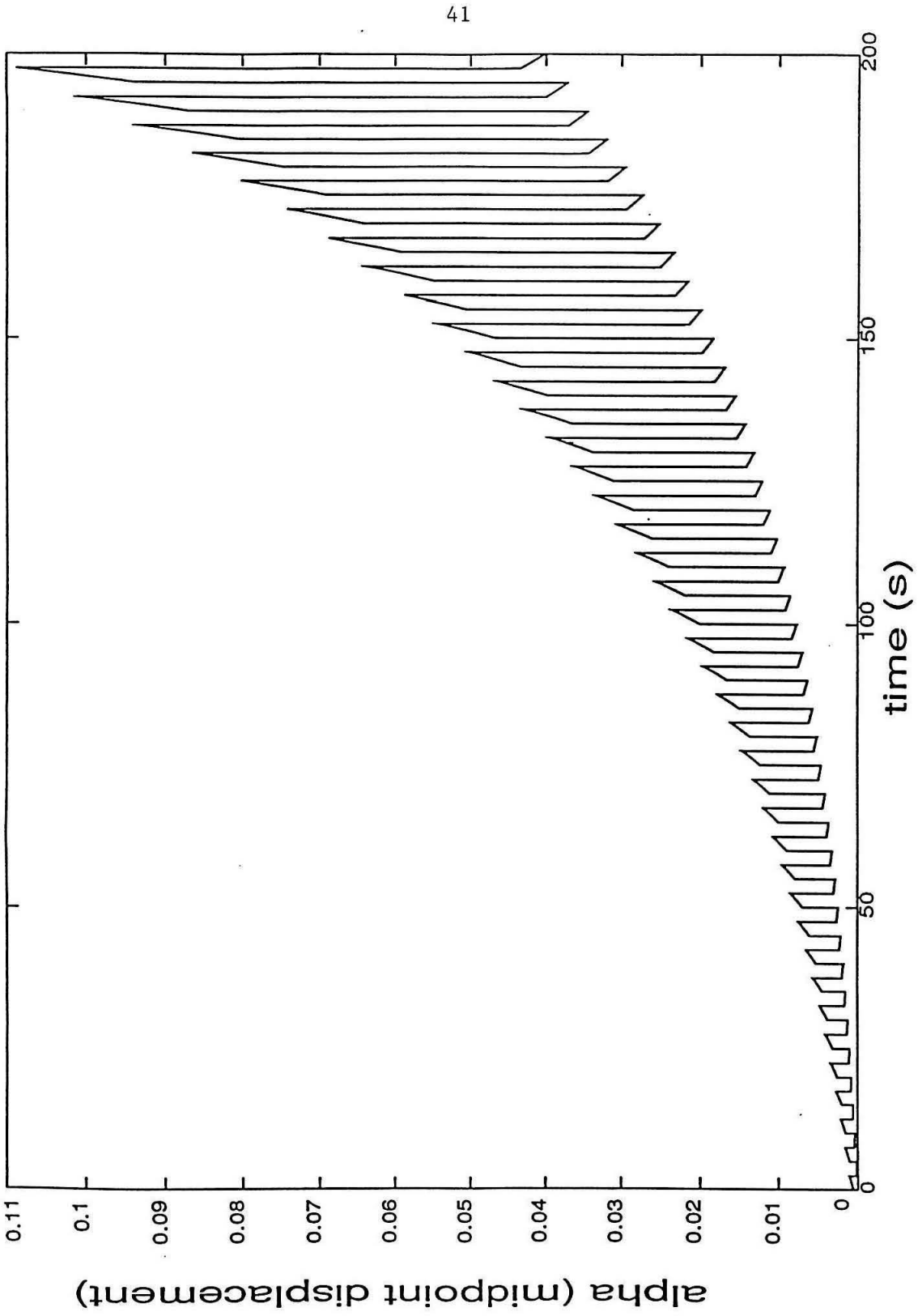


Figure 9

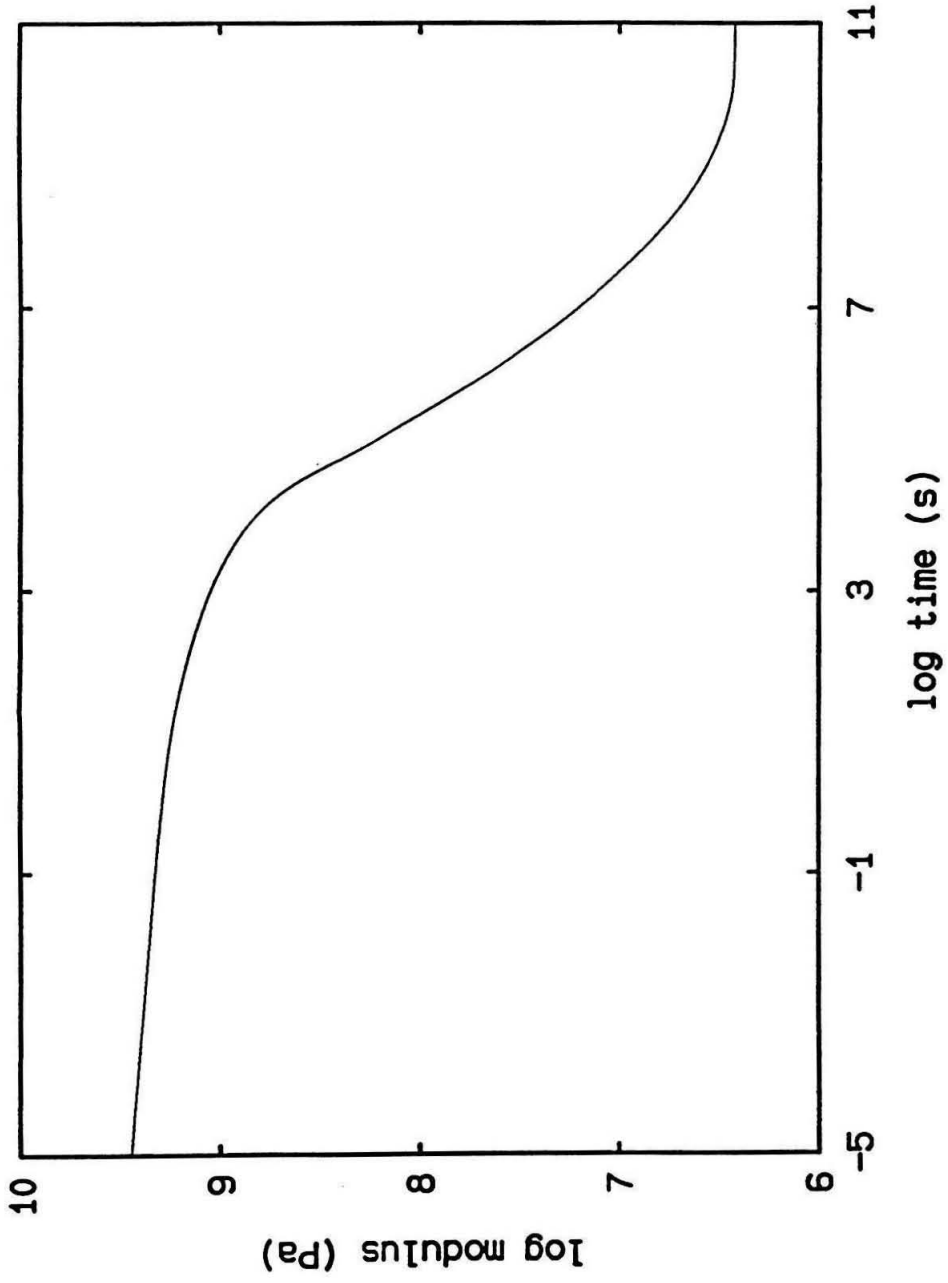


Figure 10

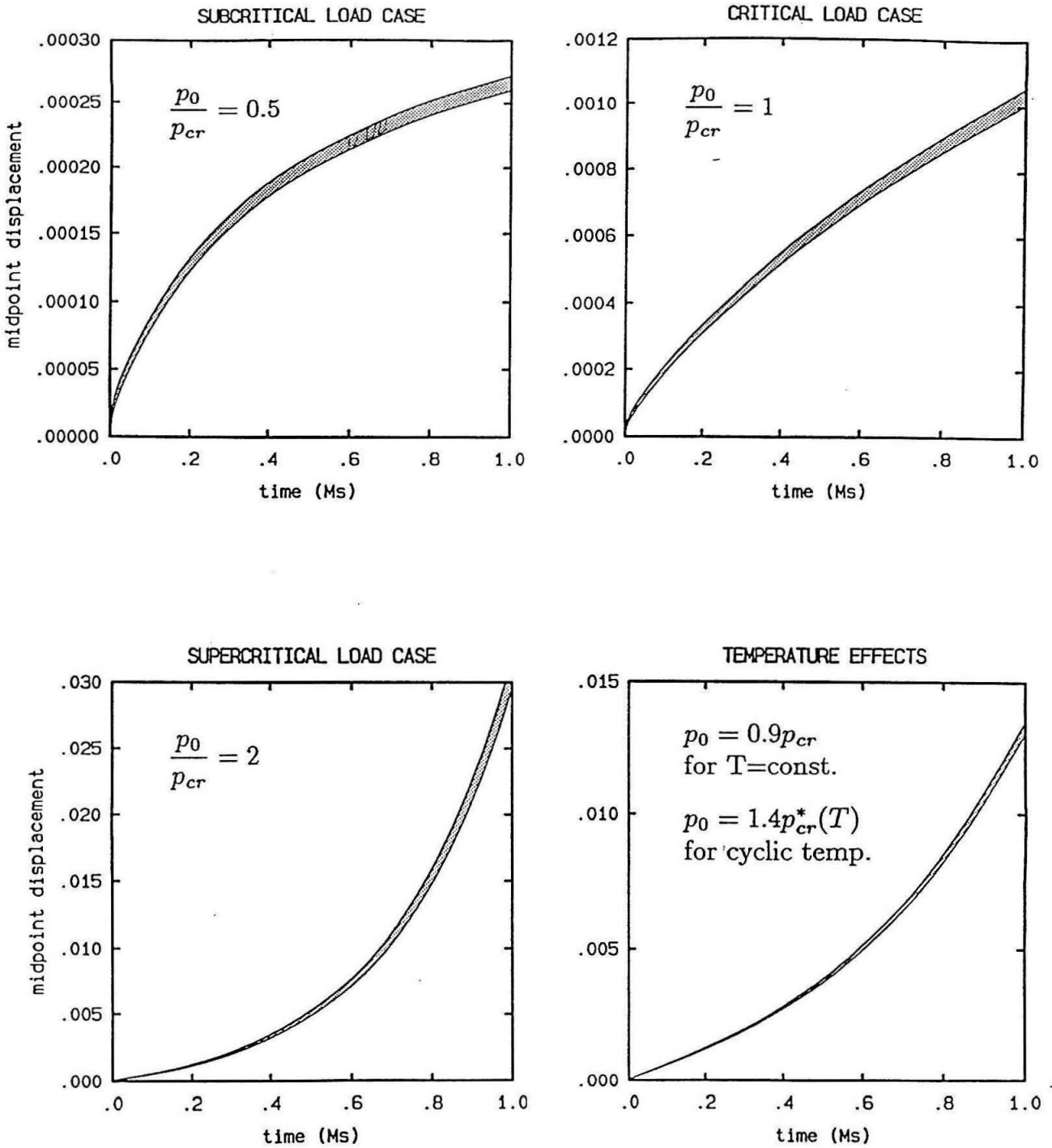


Figure 11

Comparison of Cyclic and Constant Loadings

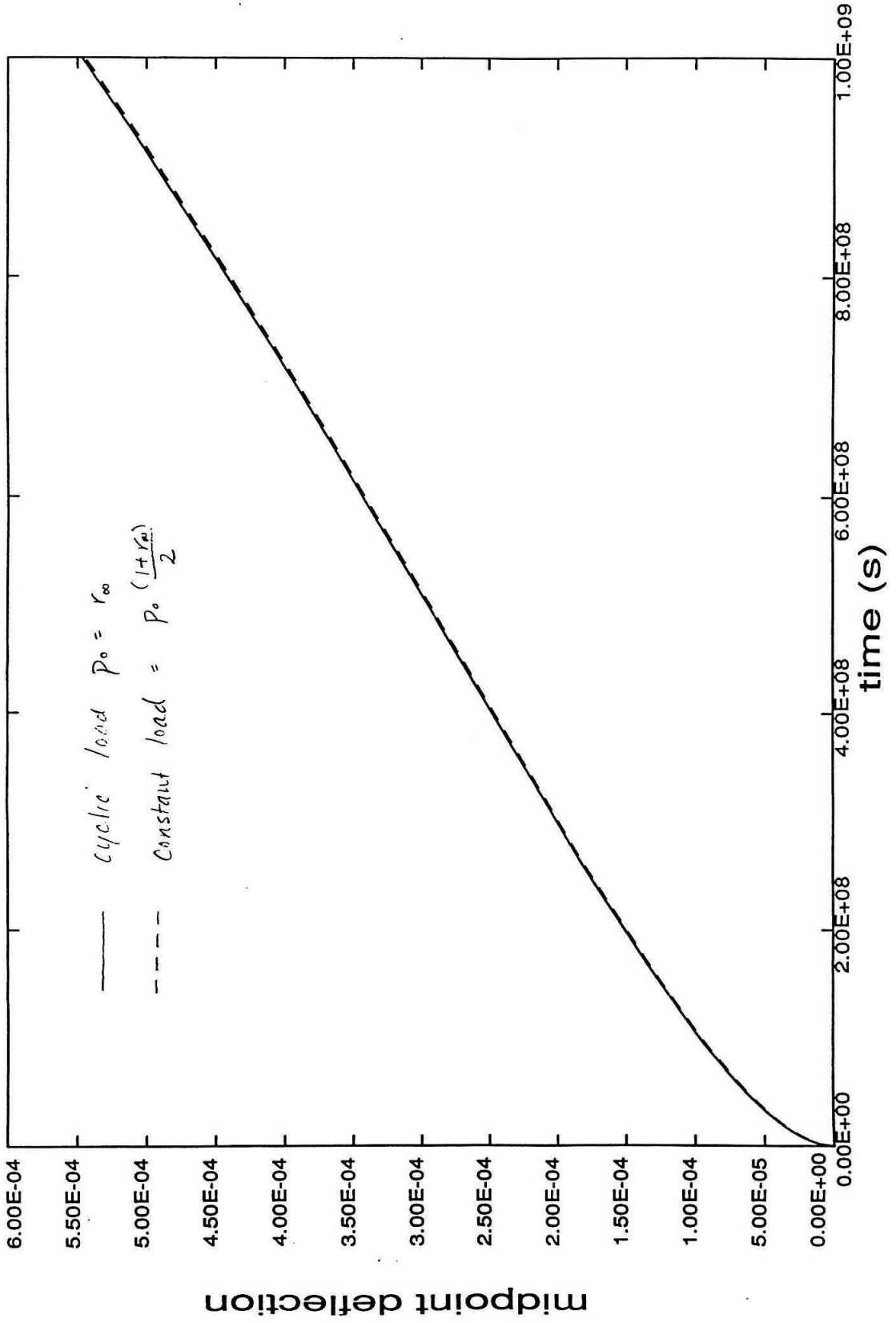


Figure 12

Comparison of Cyclic and Constant Loadings

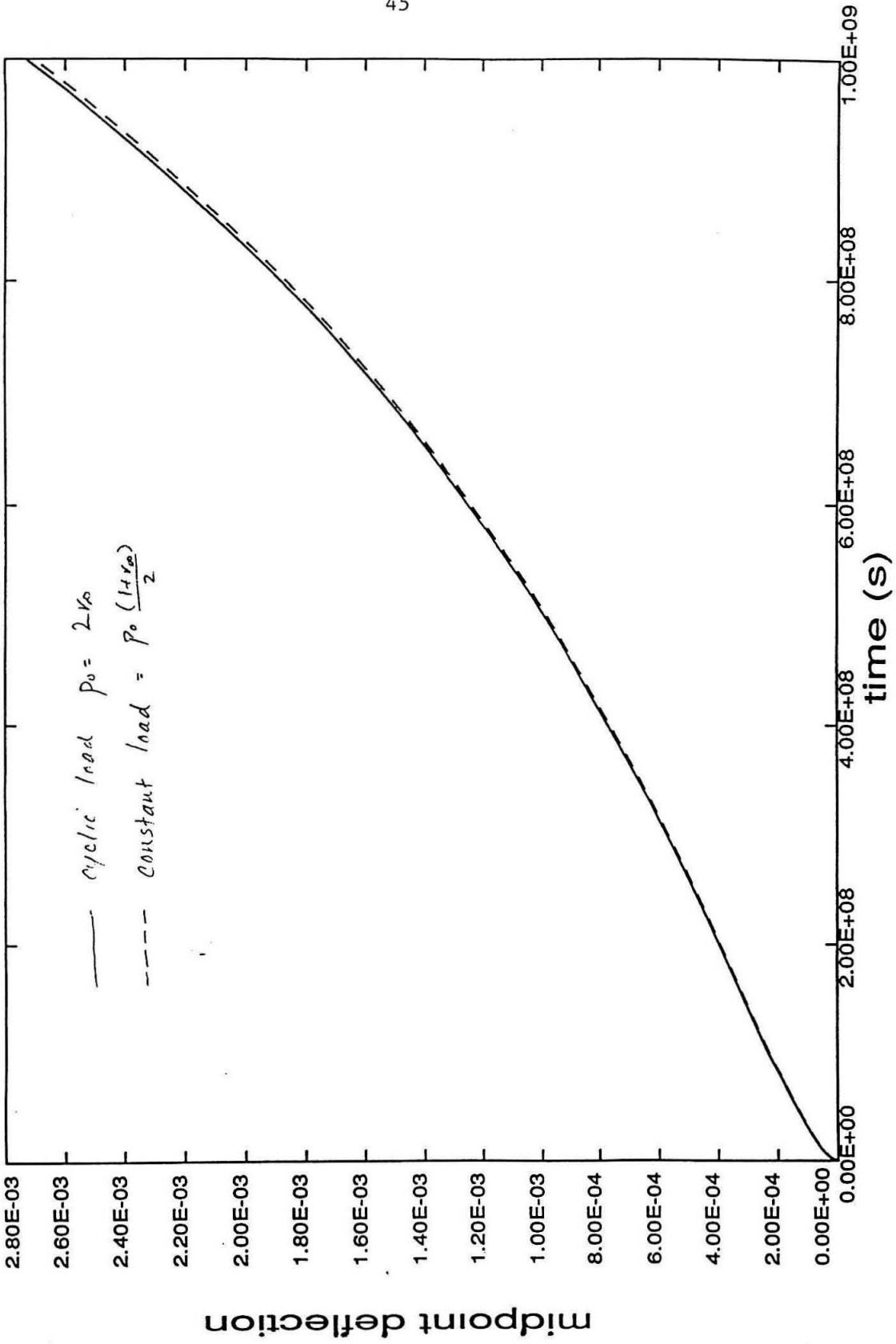


Figure 13

Comparison of Cyclic and Constant Loadings

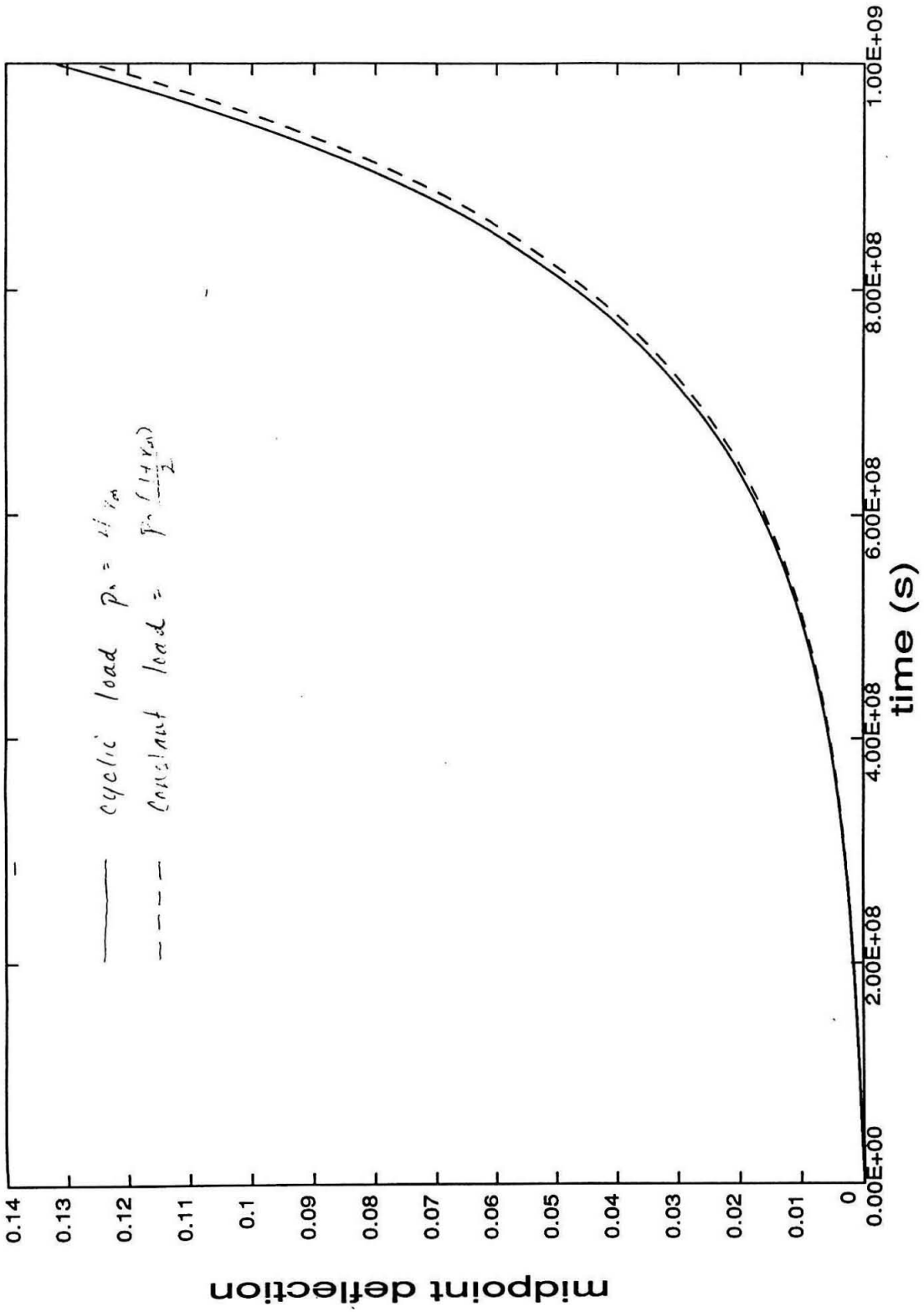


Figure 14

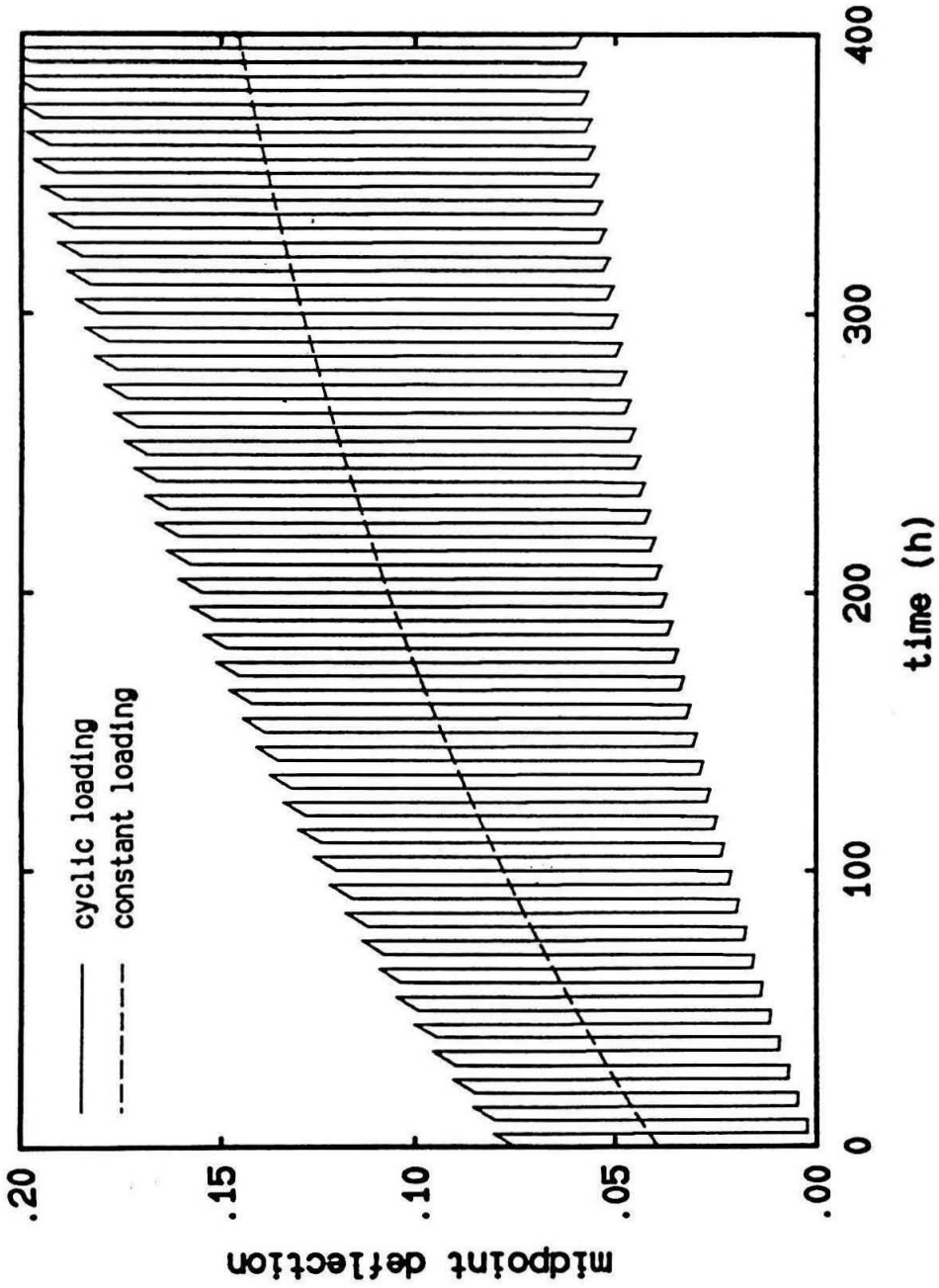


Figure 15

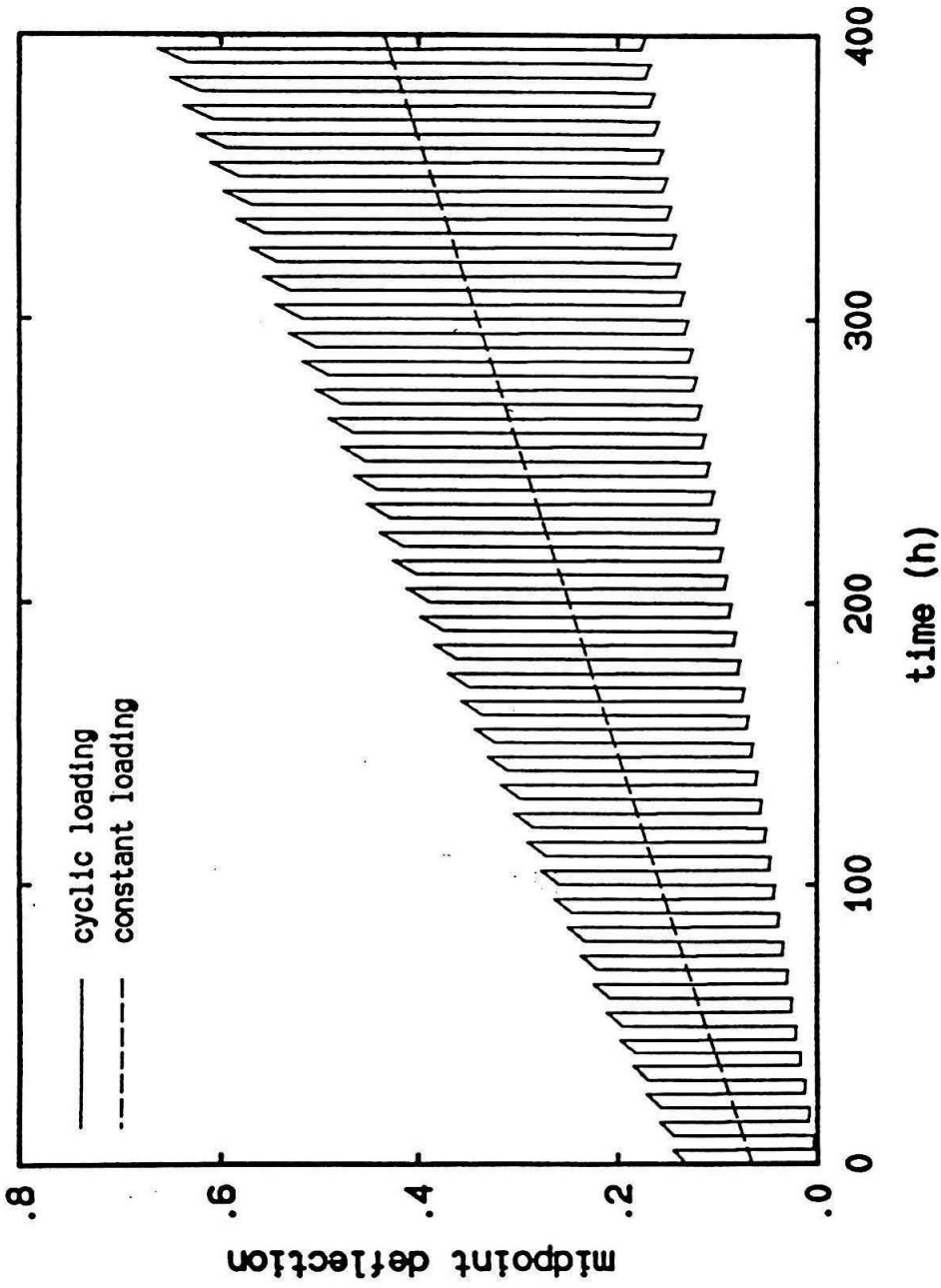


Figure 16

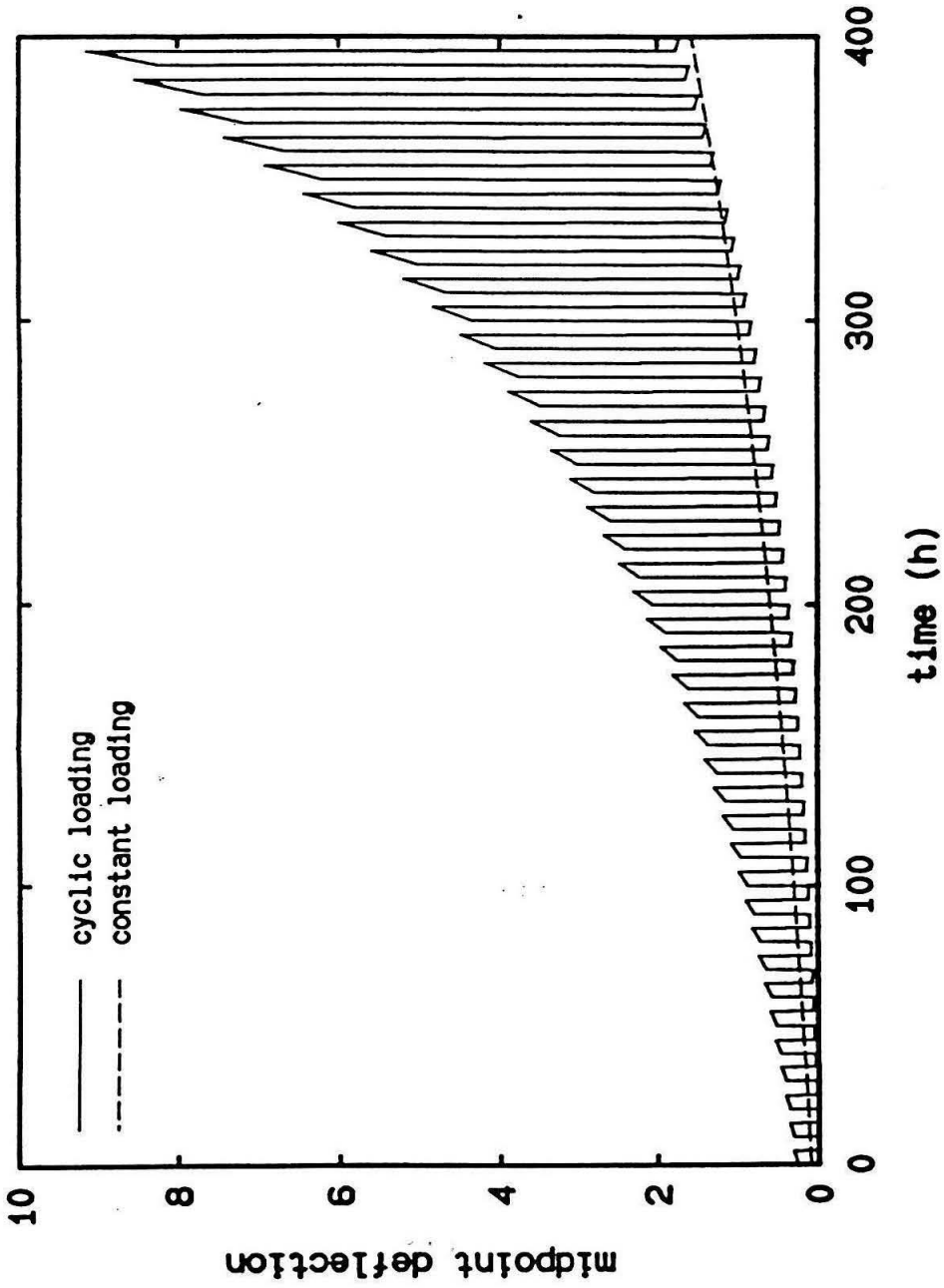


Figure 17

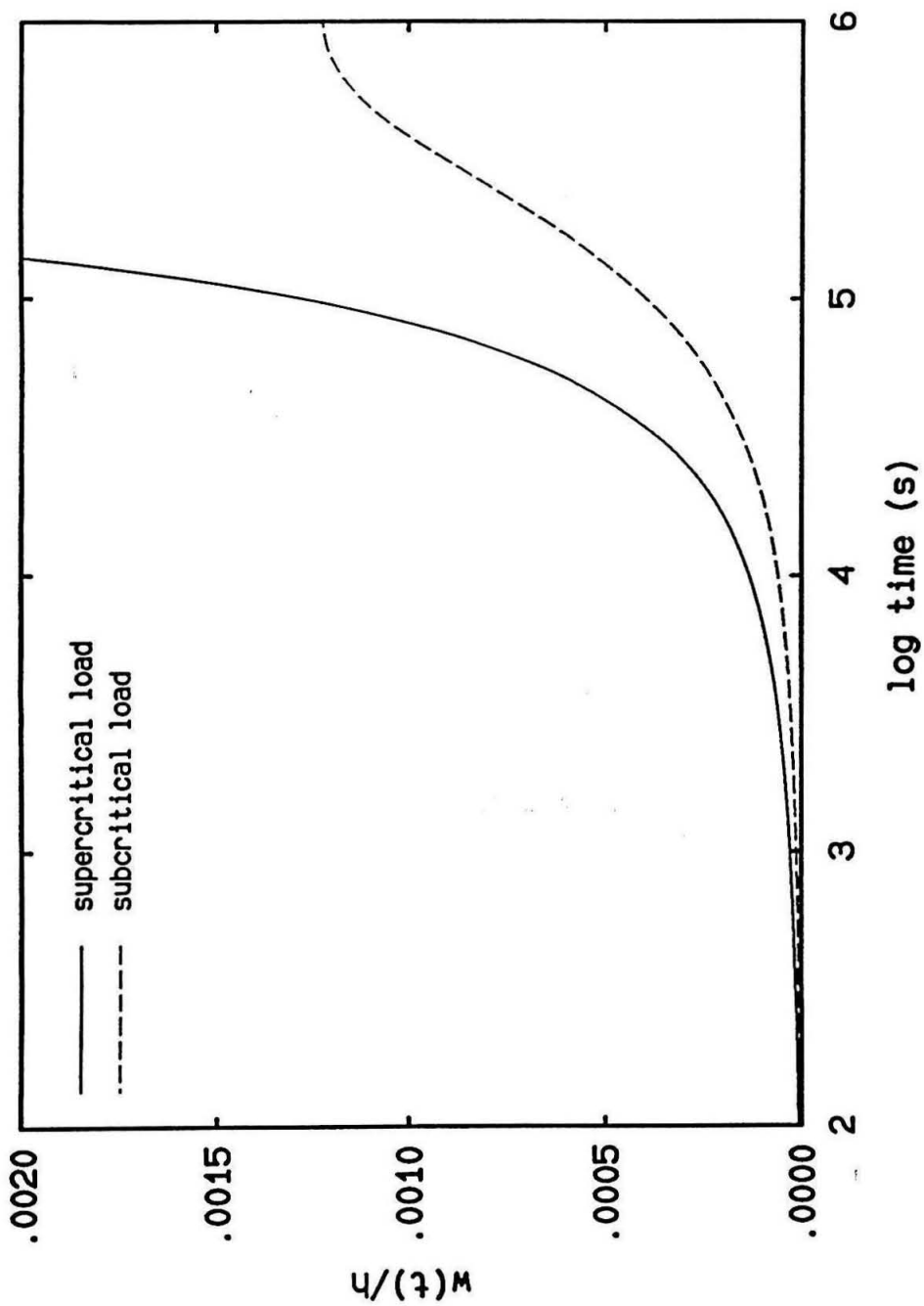
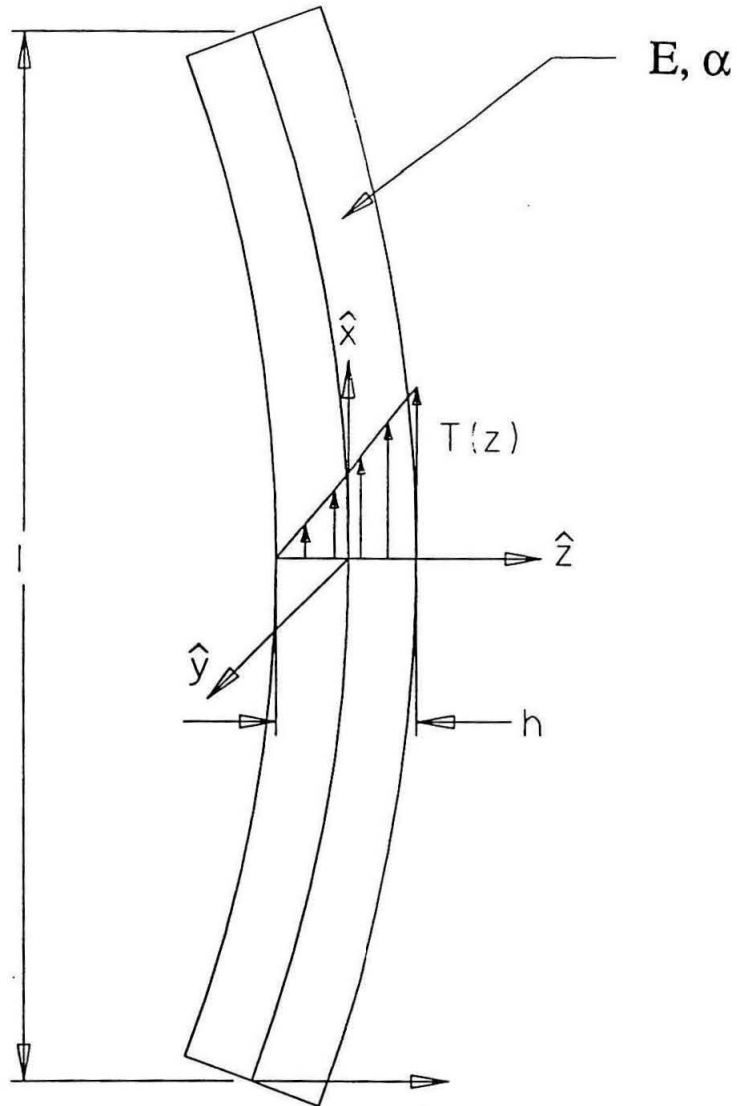


Figure 18

**Figure 19**

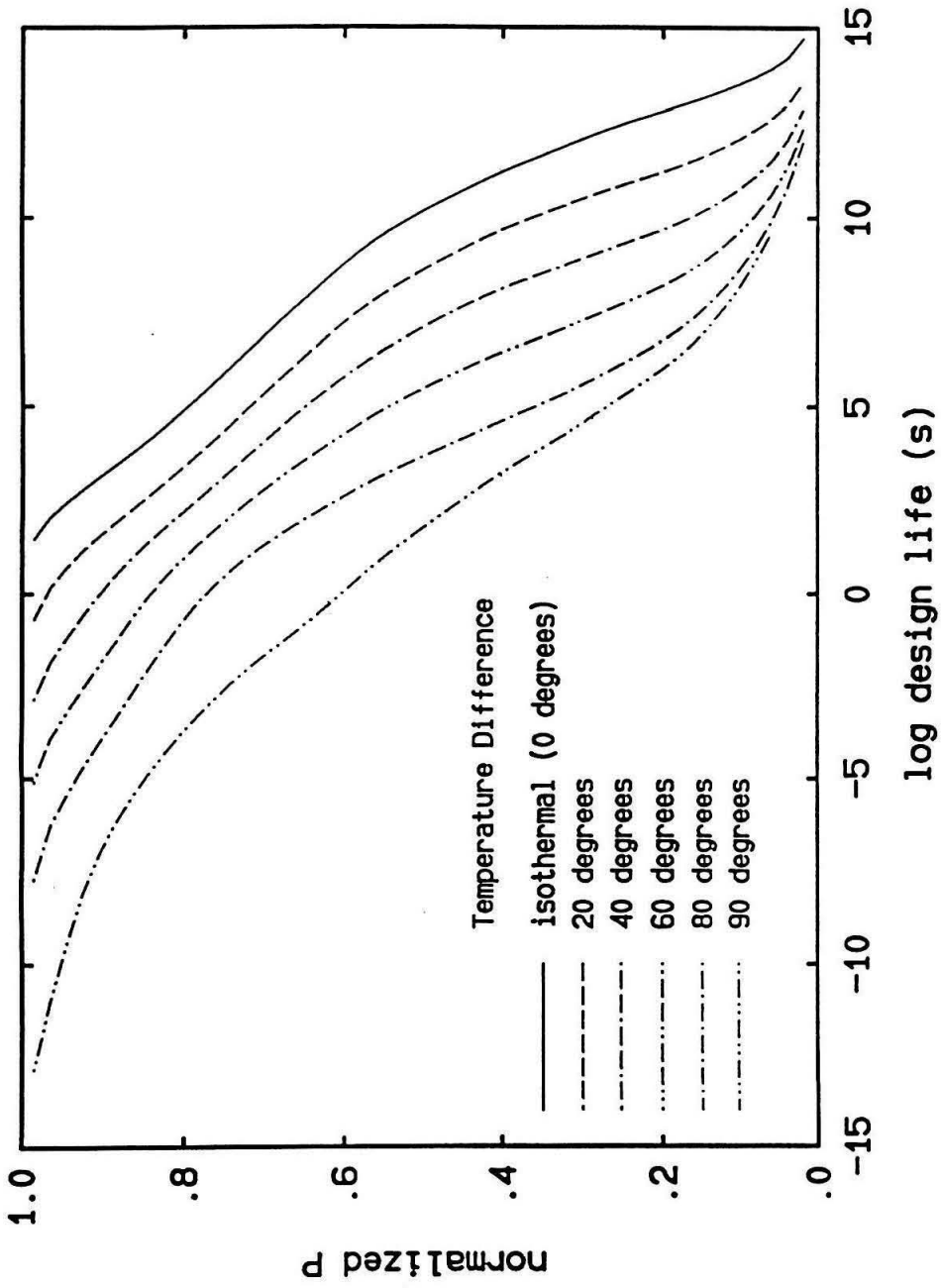


Figure 20

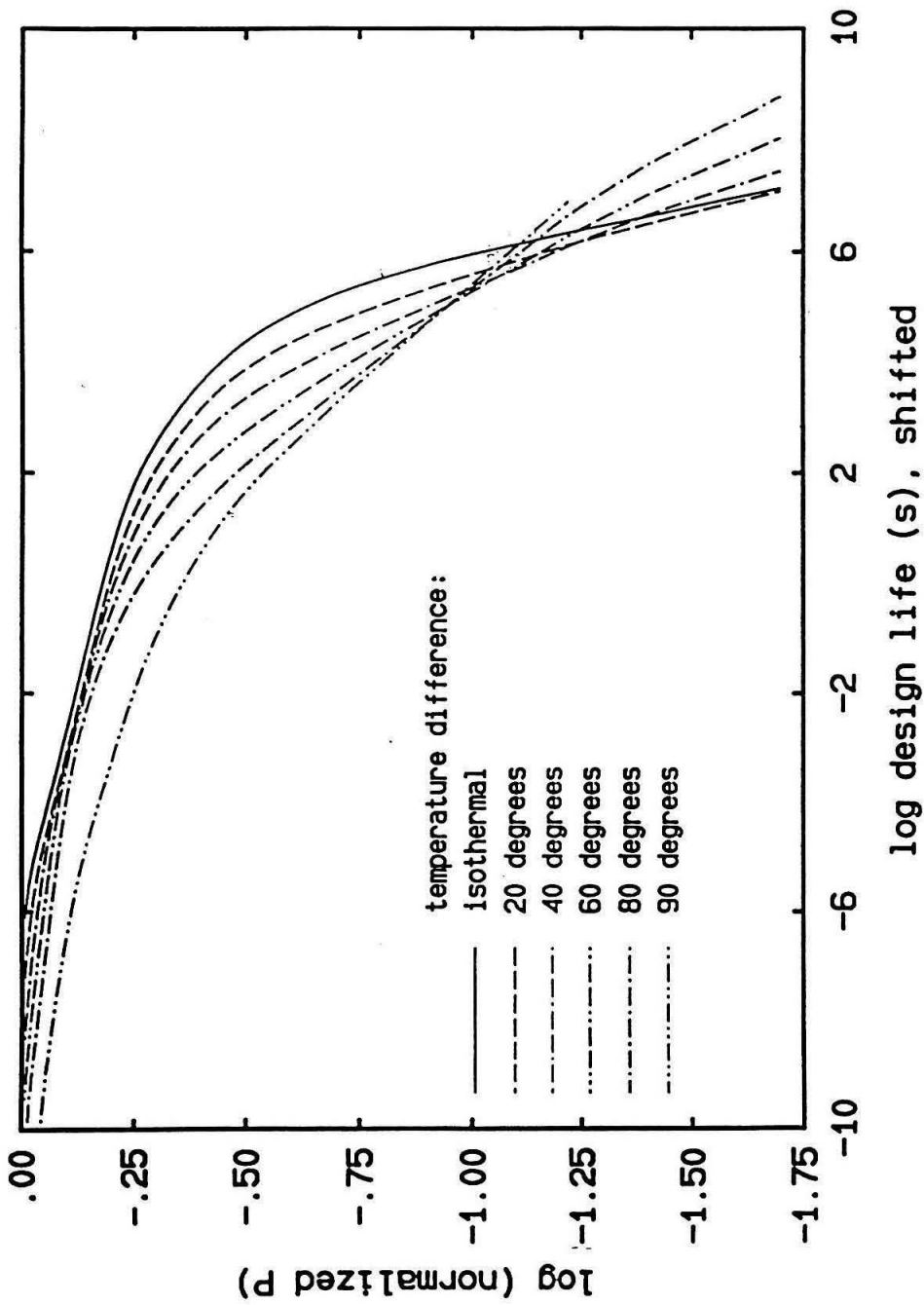


Figure 21

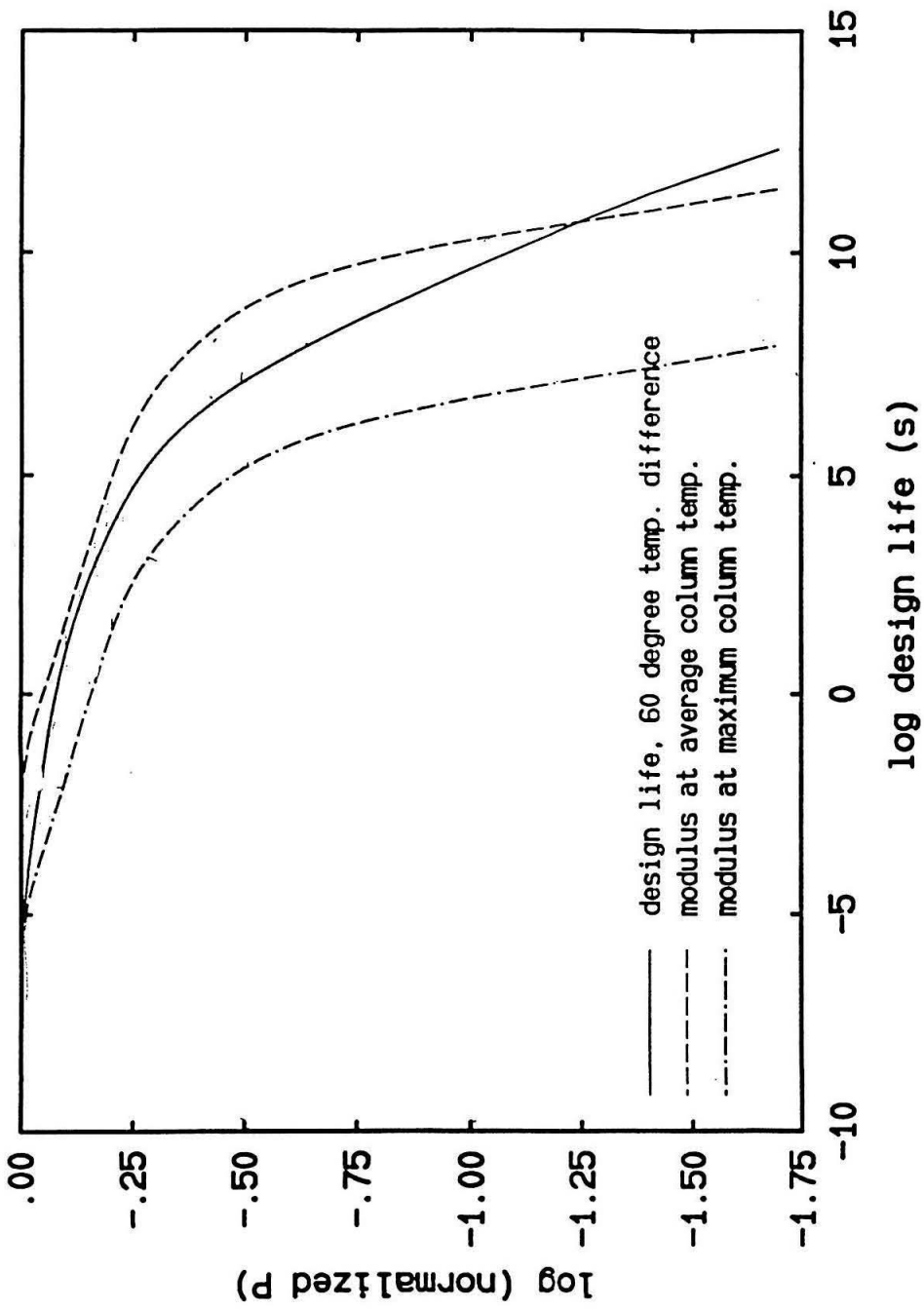


Figure 22